Scout-2 HydroGNSS - L1 Algorithm Theoretical Baseline Document (ATBD)

Project:	**Scout 2 HydroGNSS**
SSTL Reference:	00655831
Customer Reference:	4000135686/21/NL/AD
Release Number:	12.0
Release Date:	21/01/2026
Status:	Release
Prepared By:	Tom Norris
Reviewed By:	Martin Unwin
Approved By:	Peter Garner

UK Export Control	**This document and any hardware referred to within has been UK Export Control Rated as:**	
Hardware UK Export Rating Number:	N/A [Not controlled for UK export]	**Date of rating:** 31/03/2026
Information UK Export Rating Number:	N/A [Not controlled for UK export]	
I confirm I am an approved SSTL Export Rater and this rating is correct as of the date above:		Martin Unwin
US Export Control	No US origin information	
ITAR	**The information contained herein is controlled under US ITAR and is authorised for export under the provision of TAA/DSP: N/A (Not controlled)**	
EAR	**The information contained herein is controlled under US EAR and has been classified as ECCN: N/A (Not controlled)**	
ITAR EAR	**The following statement is only applicable for documents containing ITAR/EAR classified information. This document contains information controlled by the U.S. government and authorized for export only to the country of ultimate destination for use by the ultimate consignee or end-user(s) herein identified. It may not be resold, transferred, or otherwise disposed of, to any other country or to any person other than the authorized ultimate consignee or end-user(s), either in its original form or after being incorporated into other items, without first obtaining approval from the U.S. government or as otherwise authorized by U.S. law and regulations.**	

Document Revision Status

Last Edited Date	Revision Number	Status	Edited By	Pages/Paragraph Affected	Change Ref
	1-10			Refer to previous version for historical changes.	
13/06/2025	11.0	Release	MJU, TDN	Misc review comments addressed. Slope compensation algorithm expanded, eqn corrected. swAGC described in more detail, gain control table and text expanded Channel allocation outline expanded.	Sect 3.1.3.6 Sect 3.2.4.5 Appx C Section 3.1.3.6.3
16/04/2026	12.0	Release	MJU, TDN	Updates to Receiver Power Metrics – adjusted algorithms to include sampling loss. Changes to temperature compensation for LNA and front-ends.	Section 3.2.4

TABLE OF CONTENTS

LIST OF FIGURES

LIST OF TABLES

1 INTRODUCTION

1.1 SCOPE

As part of the ESA Scout-2 HydroGNSS mission this Algorithm Theoretical Baseline Document (ATBD) captures the algorithms for each of the SSTL L1 processors; L1AOP, L1BOP and L1BOP-DX (which requires the training algorithm L1B0P-DX-L). SSTL algorithms for all datasets are part of the Payload Data Ground Segment (PDGS).

1.2 APPLICABLE DOCUMENTS

Applicable Documents identified in the following text are identified by AD-n, where "n" indicates the actual document, from the following list:

AD#	Title	Doc #	Revision	Date
AD-1	HydroGNSS PDGS Algorithm ICD	SP#00637207	20	11/03/2026
AD-2	Scout-2 HydroGNSS Mission Requirements Definition	SP#00632438	3.0	26/02/2024
AD-3	Scout 2 HydroGNSS Calibration/Validation Plan	SP#00644845	10.0	08/10/2025
AD-4	Scout-2 HydroGNSS - GNSS Satellite Transmission Characteristics	SP# 00663870	4.0	22/07/2024
AD-5	Scout-2 HydroGNSS – Scientific Requirement Flow down and Error Allocation	SP# 00672665	5.0	22/07/2024
AD-6	Technical Note – Geolocation on the HydroGNSS Mission	SP# 00722877	1.0	05/07/2024

1.3 REFERENCE DOCUMENTS

Documents referenced in the following text, are identified by RD-n, where "n" indicates the actual document, from the following list:

RD#	Title	Customer Rf#	SSTL Doc #	Revision	Date
RD-1	Network Common Data Form (netCDF) http://www.unidata.ucar.edu/software/netcdf/			4.8.1	23/08/2021
RD-2	Surface Soil Moisture ATBD		SP#00649693	2.9	10/06/2025
RD-3	Freeze/Thaw State ATBD		SP#00649720	3/1	08/11/2024
RD-4	Inundation/Wetlands ATBD		SP#00649719	4.7	12/11/2024
RD-5	Forest Above Ground Biomass ATBD		SP#00655639	1.6	10/05/2025
RD-6	Ocean Wind Speed and Ice Extent ATBD		SP#00654815	1.1	16/12/2022
RD-7	CYGNSS ATBD L1B DDM Calibration		148-0137	4	09/11/2021
RD-8	ITU-R – Attenuation by atmospheric gases		ITU-R P.676-11		Sept 2016
RD-9	GNSS Antenna Characterisation – Final Report and Abstract	4000122597/17/NL	SSHC-0326172	001	19/12/2018
RD-10	HydroGNSS E2ES ATBD		00655850	2.1	20/06/2024
RD-11	MERRByS Product Manual - GNSS Reflectometry on TDS-1 with the SGR-ReSI		ST#0248366	7	02/01/2019
RD-12	SGR ReSI User Manual (CYGNSS)		ST#0216897	8	02/08/2016
RD-13	NOC Level 1B_Ext Processor ATBD		SP# 00654816	1	18/05/2022
RD-14	HydroGNSS Reference Frame Definition Document		SP# 00649629	1	11/08/2022
RD-15	MERRByS Product Manual - GNSS Reflectometry on TDS-1 with the SGR-ReSI		ST#0248366	7	02/01/2019

RD-16	Scout-2 HydroGNSS L1BOP-DX-L Antenna Learning User Manual		SP# 00696930	0.28	04/06/2024

1.4 REFERENCE LITERATURE

Danielson, J.J., and Gesch, D.B., 2011, Global multi-resolution terrain elevation data 2010 (GMTED2010): U.S. Geological Survey Open-File Report 2011–1073, 26 p.

Gordon W. B., "Reflections from Multiple Surfaces Without Edges," in *IEEE Transactions on Antennas and Propagation*, vol. 58, no. 10, pp. 3222-3230, Oct. 2010, doi: 10.1109/TAP.2010.2055785.

Hajj, G & Zuffada, C. (2003). Theoretical description of a bistatic system for ocean altimetry using the GPS signal. Radio Science - RADIO SCI. 38. 10-1. 10.1029/2002RS002787.

Hegarty C, “Analytical Model for GNSS Receiver Implementation Loss”, Navigation: Journal of the Institute of Navigation, Vol 58, No 1, Spring 2011.

Jales. (2015). Spaceborne receiver design for scatterometric GNSS reflectometry [University of Surrey]. https://openresearch.surrey.ac.uk/discovery/delivery/44SUR_INST:44SUR_VU1/12138629250002346

King L, M. Unwin, J. Rawlinson, R. Guida and C. Underwood, "A Topographically-Accurate GNSS-R Reflection Point Predictor for on-Board Operational Processing," *IGARSS 2020 - 2020 IEEE International Geoscience and Remote Sensing Symposium*, 2020, pp. 6194-6197, doi: 10.1109/IGARSS39084.2020.9324677.

Martin-Neira, M. A passive reflectometry and interferometry system (PARIS): Application to ocean altimetry. ESA J. 1993,17, 331–355.

Slater, Shepherd, McMillan, Muir, Gilbert, Hogg, Konrad and Parrinello: A new digital elevation model of Antarctica derived from CryoSat-2 altimetry, The Cryosphere, 2018. DOI 10.5194/tc-12-1551-2018.

Wang T., *et al*., "Dynamic Calibration of GPS Effective Isotropic Radiated Power for GNSS-Reflectometry Earth Remote Sensing," in *IEEE Transactions on Geoscience and Remote Sensing*, vol. 60, pp. 1-12, 2022, Art no. 5800512, doi: 10.1109/TGRS.2021.3070238.

Wang T., C. S. Ruf, B. Block, D. S. McKague and S. Gleason, "Design and Performance of a GPS Constellation Power Monitor System for Improved CYGNSS L1B Calibration," in *IEEE Journal of Selected Topics in Applied Earth Observations and Remote Sensing*, vol. 12, no. 1, pp. 26-36, Jan. 2019, doi: 10.1109/JSTARS.2018.2867773.

1.5 ACRONYMS AND ABBREVIATIONS

The following abbreviations are used within this document:

ADC	Analogue to Digital Conversion
AGB	Above Ground Biomass
AGSP	Antenna Gain towards Specular Point
ANN	Artificial Neural Network
AOCS	Attitude and Orbit Control Subsystem
ATBD	Algorithm Theoretical Baseline Document
AWS	Amazon Web Services
C/A	Coarse Acquisition
CCI	Climate Change Initiative
CM#1,2,3	Calibration Method 1, 2, 3
DC	Digital Conversion
DDMStream	Proprietary format for DDM file
MOC	Mission Operations Centre
MPS	Mission Planning System
MRD	Mission Requirements Document
NBRCS	Normalized Bistatic Radar Cross Section
NASA	National Aeronautics and Space Administration
NDVI	Normalized Difference Vegetation Index
netCDF	Network Common Data Form
NORAD	North American Aerospace Defense Command
NOC	National Oceanography Centre (UK)
O/S	Operating System
PDGS	Payload Data Ground Segment
PPS	Pulse Per Second

DEM	Digital Elevation Map	PRN	Pseudo Random Noise (GPS and Galileo satellite identifier)
DR	Data Recorder	PVT	Position, Velocity and Time
DRT	Data Recorder Track	QF	Quality Flag
DTM	Digital Terrain Model	RC	Raw Collection
EASE	The Equal-Area Scalable Earth	RD	Receiver Data
E2ES	End-to-End Simulator	RF	Radio Frequency
ECEF	Earth-Centred Earth-Fixed	RFI	Radio Frequency Interference
EIRP	Effective Isotropic Radiated Power	RINEX	Receiver Independent Exchange Format
EWOD	Extended Whole Orbit Data	SBPP	SGR Binary Packet Protocol
F-AGB	Forest Above Ground Biomass	SGR	Space GNSS Receiver
FDI	Fast Delivery Inversion	SMAP	Soil Moisture Active Passive (NASA mission)
FMI	Finnish Meteorological Institute	SMOS	Soil Moisture and Ocean Salinity (ESA mission)
FT	Freeze Thaw	SNR	Signal to Noise Ratio
GLDAS	Global Land Data Assimilation System	SOC	Spacecraft Operations Centre
GMF	Geophysical Model Function	SP	Specular Point
GNSS	Global Navigation Satellite System	SSM	Surface Soil Moisture
GL	GNSS Log (Payload file)	SSTL	Surrey Satellite Technology Limited
GSID	GNSS-R Sea Ice Detection	SV	Space Vehicle (GNSS satellites)
HSI	High-Speed Interface	SVN	Space Vehicle Number
IEEC	Institut d'Estudis Espacials de Catalunya	swAGC	Software-Controlled Automatic Gain Control
IF	Intermediate Frequency	TBC	To Be Confirmed
IFAC	Istituto di Fisica Applicata Nello Carrara	TBD	To Be Defined
IGBP	International Geosphere-Biosphere Programme	TLE	Two-Line Elements
IGS	International GNSS Service	VM	Virtual Machine
L1OP	Level 1 Operational Processor	VOD	Vegetation Optical Depth
L1PP	Level 1 Prototype Processor	WOD	Whole Orbit Data
L2OP	Level 2 Operational Processor	WST	SSTL-proprietary satellite data format
L2PP	Level 2 Prototype Processor	ZTC	Zoom Transform Correlator (On-board processing algorithm)
MERRByS	Measurement of Earth Reflected Radio-navigation Signals By Satellite		

1.6 DEFINITIONS

Ancillary Data. Data generated on-board in support of the observation data, both by the instrument and the platform, such as, navigation, temperature, attitude, Housekeeping Telemetry (HKTM), timing data and configuration. When generated by the instrument they are called “instrument ancillary” when by the platform “platform ancillary”.

Auxiliary Data. In the ground segment this is the data needed to perform ground processing and not part of the measurement data set generated on board (this might include e.g. pre-launch calibration data and Land Cover database).

Channel. A channel is used to designate a ZTC Delay Doppler Map generating unit. In the nominal case there are 16 channels made up by four different RF configurations (L1 LHCP, L1 RHCP, L5 LHCP, L5 RHCP), targeting four separate GNSS reflection tracks. Each channel can generate incoherent DDM and coherent measurements.

CM#1,2,3 Calibration Methods for estimating EIRP from GNSS satellites. CM#1 models EIRP from published, learnt antenna patterns and past power data, CM#2 fits average powers over ocean, and CM#3 corrects EIRP dynamically using directly received signals when available.

2 PROCESSING OVERVIEW

HydroGNSS Level 1 processors are defined in AD-1, the utilised algorithms are captured in this document. Figure 2.1 shows the processors in the PGDS context: L1AOP, L1BOP, L1BOP-DX (which requires the training algorithm L1BOP-DX-L).

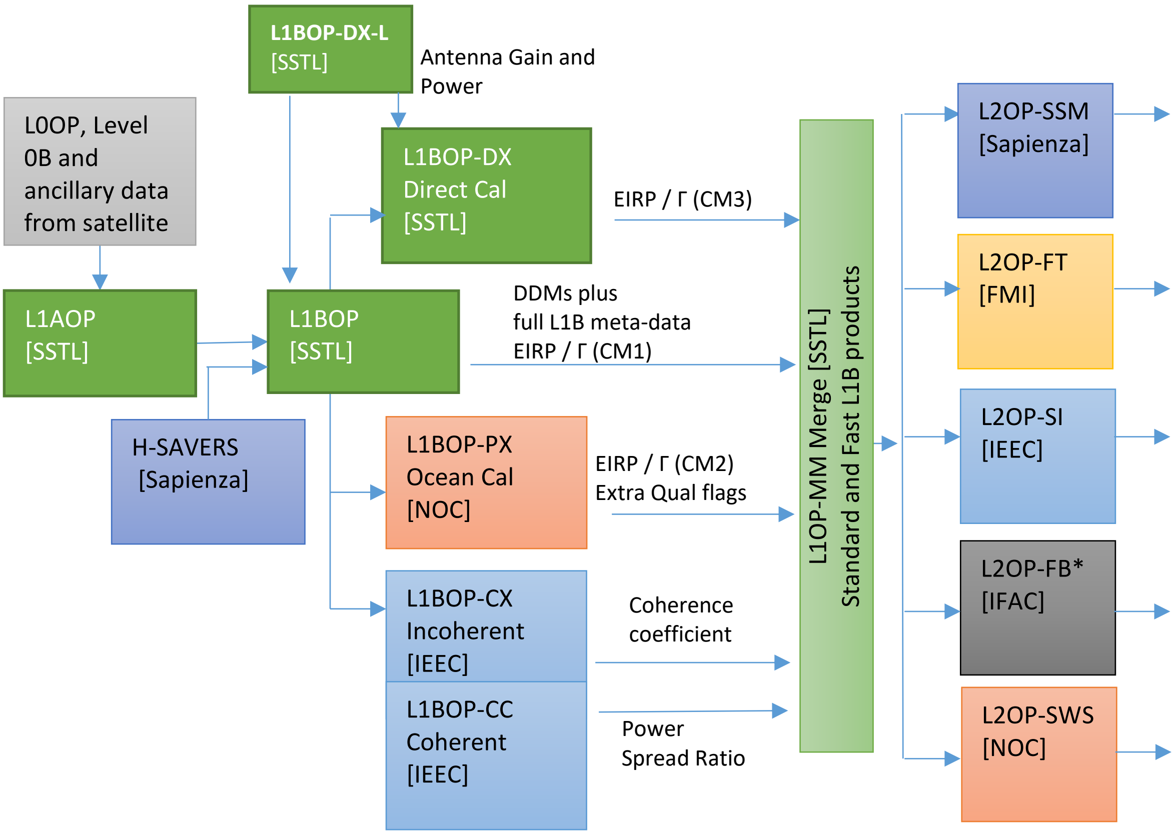

Figure 2.1 Level 1 processors in context of PDGS

2.1 PROCESSING OUTLINE

The inputs to the main PDGS processing chain are the L0b payload data files, GL logs, AOCS logs and (Whole Orbit Data) WODs downloaded from the satellite. In addition, orbital elements of the GPS and Galileo satellites, topographic data consisting of global Digital Elevation Maps (DEMs), and on-board antenna parameters are used to generate metadata.

An SSTL L1a processor will process the level 0b Doppler Delay Maps (DDMs) into a standard level 1a NetCDF format, and generate L1a metadata files collated from GNSS files, GL logs, and WODs.

An SSTL L1b core processor will generate metadata including radiometric corrections based on the black body nadir and zenith sources, include data quality flags and EIRP estimation (known as CM#1), to form the level 1b core metadata that includes reflection and bi-static scattering coefficients.

A L1BOP-DX provides further metadata and calculates GNSS satellite transmitter power corrections, using zenith antenna measurements of direct signals from the GNSS satellites (this forms the EIRP CM#3 method). This functionality has been incorporated into L1BOP, so there is no separate L1BOP-DX module.

A NOC L1b_ext processor will in parallel generate metadata including a posteriori GNSS transmitter power corrections and HydroGNSS receiver gain corrections, using calibration data from HydroGNSS ocean data. The NOC L1b processor will also generate quality flags.

The training module (L1BOP-DX-L) is used to determine GNSS satellite antenna patterns and transmit powers, intended for calibration methods CM#1 and CM#3.

2.1.1 L0b Summary

The L0b DDMs are processed on-board from data samples (equivalent to Level 0a), from nominally 4 simultaneous reflection tracks (a consecutive sequence of reflections at a specular point). Reflection tracks can be from GPS or Galileo. For each of the four allocated tracks there are a maximum of four DDM channels observed (L1/E1 LHCP, L5/E5A LHCP, L1/E1 RHCP and L5/E5A RHCP), each with incoherent and coherent measurements. The allocation algorithm used on the instrument (see Appendix C: for outline) selects reflections to track based on the L1-band antenna gain towards the specular point (AGSP), on the assumption that a higher antenna gain will result in a better estimation of the scattering cross-section at the surface.

2.1.2 Processor Data Types

The extent of the processing of each data type is captured in Table 2-1.

Table 2-1 Data Types Processed by L1a and L1b Operational Processors

Reflection Channels / Processor	E1/L1 LHCP DDM	E1/L1 RHCP DDM	E5A/L5 LHCP DDM	E5A/L5 RHCP DDM	Comments
L1AOP	Y	Y	Y	Y	
L1BOP	Y	Y	Y	Y	All data processed, even if some reflected signals may be too weak for useful outputs
L1BOP-DX	Y	N	N*	N	* Direct E5 / L5 acquisition not currently implemented, direct signal unavailable for LHCP calibration. (No mechanism for in-orbit RHCP calibration available.)
L1BOP-DX-L	Y	N	N*	N	As above, however transmit patterns and powers can be obtained from published data, or generated through processing alternate data sources (Sentinel-6a for example)

2.1.3 Notes about L0P and L1OP-MM Processors

These two processors are file handlers and do not require ATBD description, but their functions are summarised here.

L0-OP – Splits HSI (High-Speed Interface) files downloaded from HydroGNSS satellite(s) into L0a raw GNSS-R files and L0b DDMs in SSTL proprietary formats. L0A are converted into integer files for each RF channel that can be read by the PGDS. L0B files are reconstructed from the HSI files, undoing the on-board variable compression.

L1OP-MM – Populates L1a, L1b core, and L1b_ext metadata into single files for use by Level 2 processors.

3 ALGORITHM DESCRIPTION

3.1 L0B TO LEVEL 1A (L1AOP)

The SSTL level 1a processor (L1AOP) processes the L0b into L1a netCDF format. L1AOP also generates L1a metadata containing all relevant instrument and platform ancillary data. The processing flow takes the on-board processed DDMs and converts them into DDM products with synchronised metadata derived from the payload data and EWODs and SBPP file.

Table 3-1 L0b to L1a processing

Type	Data	Format	Note
Inputs:	L0b on-board processed DDMs and coherent measurements, extracted from the payload data into an SSTL proprietary format, including up to 16 DDM/coherent channels.	DDMStream	See HydroGNSS PDGS Algorithm ICD [AD-1]
Ancillary data (Payload):	Receiver status and PVT from GL log file	SBPP	
Ancillary data (Platform):	AOCS Logs, WOD data containing satellite attitude	WST	
Auxiliary data:	Broadcast GNSS Ephemeris Broadcast GNSS Ionospheric Parameters DEM and Geoid files, consistent with the file used on-board satellite	RINEX Navigation Data RINEX Navigation Data *.TIFF	
Outputs:	**L1a DDM** Original Size 128 delay lines x 20 Doppler, now reduced to 52 x 20. Nominal sampling 53 MHz, 18.87 ns, 5.661 metres. L1 Delay Spacing: 226.4 ns (67.93 m) L5 Delay Spacing: 75.48 ns (22.64 m) Doppler spacing: 125 Hz for 4 ms, 500 Hz for 1 ms.	*.netCDF, 1Hz DDM 52 delay lines, 20 Doppler lines x No. Of chans	See HydroGNSS PDGS Algorithm ICD [AD-1]
	Coherent Measurements	Coherent :(250Hz I,Q, 3 pixels x No. Chans)	
	Metadata (metadata_1a.nc) generated from the payload and platform data: Specular Point (Angles, X, Y, Z, Lat, Lon, H) DDMOutputNumericalScaling Flags Payload & Platform Data (incl. temperatures)	*.netCDF, 1Hz	
	blackbodyZenithL5E5.nc blackbodyZenithL1E1.nc blackbodyNadirL1E1LHCP.nc blackbodyNadirL1E1RHCP.nc blackbodyNadirL5E5LHCP.nc blackbodyNadirL5E5RHCP.nc	*.netCDF	
	directSignalPowerL1E1.nc directSignalPowerL5E5.nc	*.netCDF, 1Hz	

3.1.1 Theoretical Description

The following sections provides an outline of the L1AOP processing pipeline.

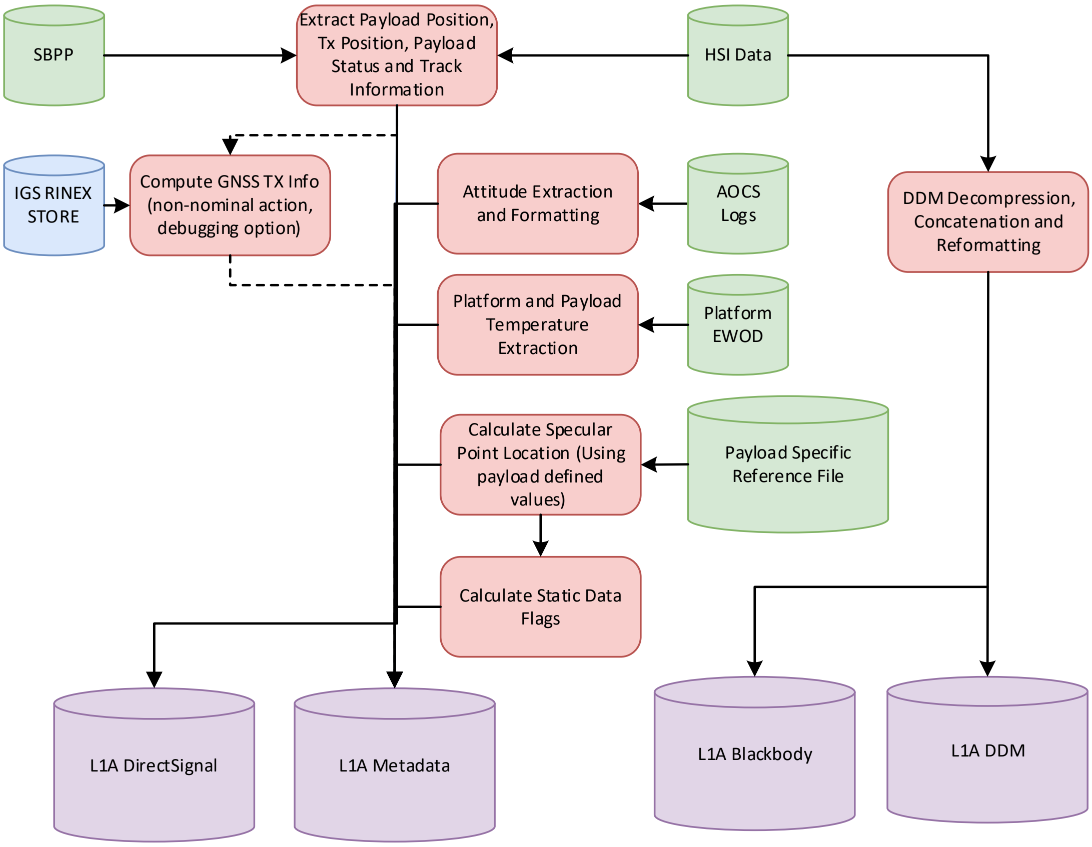

Figure 3.1 L1a Processing

3.1.2 Data Extraction

The L0b to L1a processing task takes L0b DDMs which are split out from the High-Speed Interface (HSI) files by the L0P process. Each DDM is taken in turn and using the L1a DDM Track Headers and GL log data (payload ancillary), the data is split into individual reflections. Each track is a series of individual reflections that correspond to the same transmitter PRN and the same receiver processing settings. As the receiver has up to 16 reflection channels, DDMs will be added to nominally 4 separate tracks simultaneously. HydroGNSS will use two frequencies for GPS/Galileo satellites, L1/E1 and L5/E5A (where transmitted), and two polarisations (co- and cross-polarisation), this means potentially 16 DDM channels for HydroGNSS. In addition, coherent data is included in each DDM channel. However, it may be that the L5/E5A frequencies are not used, and only the primary polarisation is used, or that more than 4 simultaneous reflections are used. NB if there are 5 reflections, then some of the dual frequency and / or dual polarisation channels will need to be deallocated, as the maximum number of channels is limited to 16. See Appendix C: for an outline of the channel allocation scheme. The L1a processor will have to detect the availability of channels from the Track Headers, process the L0b data, and construct the L1a products accordingly.

The DDMs and coherent measurements are saved to a netCDF4 file **DDMs.nc** and all the metadata is stored in the corresponding **metadata_L1a.nc**. The separation of the data and metadata can reduce time to load and filter the data. There are also separate netCDF files for the zenith and nadir antenna blackbody measurement derived from the GL log, **blackbodyZenithLXEX.nc** (nominally switched into the path every 10mins for up to 5s), and **blackbodyNadirLXEXYHCP.nc** (nominally switched into the path every 100mins for up to 5s) and direct signal file: **directSignalPowerLXEX.nc**. The format of these netCDF files is described in PDGS Algorithm ICD Document [AD-1].

For each DDM the metadata is found and synchronised to the DDM epoch, which is the midpoint between the start and end of the DDMs integration period (nominally 1000 incoherent integrations are carried out to produce a new DDM per channel every second). The DDMs of all reflection points are provided at 1Hz rate in nominal processing configuration, so the metadata is produced for each of these, interpolating as necessary. Discrete metadata fields cannot be interpolated, so the previous GL log value is used. The Coherent Measurements are output at 250 Hz.

3.1.3 Geolocation of Delay Doppler Maps

The instrument calculates the location of the specular point on-board to sufficient accuracy to place the signal within the Delay Doppler Map and with the intention of placing the coherent channel close to the nominal reflection point. The Level 1a processor ensures that the information of the applied delay and Doppler is provided to allow compensation for inaccuracies in the on-board estimation. Prediction of the specular point requires knowledge of the positions of the transmitter, the receiver, and a model of the Earth's surface. The following sections describe the processes applied on the instrument.

When operating from simulated data generated by the E2ES, the processor can also alternatively make use of satellite and specular point calculations given by the E2ES.

3.1.3.1 Transmit Position

GNSS satellite locations are available to around 1 metre accuracy in real-time from broadcast ephemerides. The International GNSS Service (IGS) makes GPS and Galileo Ephemerides available near-real time over the Internet at broadcast values, and an improved accuracy, and can offer an even more accurate service several days later. The broadcast service is used to give the transmitter position consistent with the position calculation made on-board the satellite.

Nominally at L1a, the broadcast GNSS ephemerides are obtained from IGS RINEX but this can be set by configuration to make use of ephemeris collected via the HydroGNSS satellites.

3.1.3.2 HydroGNSS Orbit

For land-based GNSS scatterometry applications, the HydroGNSS satellite position accuracy required is well within the performance of the on-board GNSS receiver. The finest resolution climate variable product has a requirement of 1 km, so the receiver orbit accuracy is unlikely to be a dominant term. The instrument is based around a GNSS receiver that determines its own location to better than 10 metres in real time, and this data will be available every second as part of the GL Log. The receiver also determines the velocity to around 0.2 m/s and time to 1 microsecond.

3.1.3.3 Specular Point Location, Quasi-spherical Earth

This method was used on-board TDS but is superseded in HydroGNSS by the ellipsoidal Earth method (section 3.1.3.4) for providing the specular point solution on an ellipsoidal Earth more accurately. The Quasi-spherical method may still be used for rapid estimation of reflection points so is described here.

The L1a dataset contains an approximate specular point location calculated on-board using a quasi-spherical Earth approach to reduce processing requirements [See Jales 2015]. Using the WGS-84 reference ellipsoid, the Earth is an oblate spheroid with a large inverse flattening parameter. This means that the calculation of the specular point on the spherical Earth can be approximated by the problem for a sphere, which can be derived directly, before adjusting back to ellipsoidal geometry. The manipulation required is shown diagrammatically in Figure 3.2.

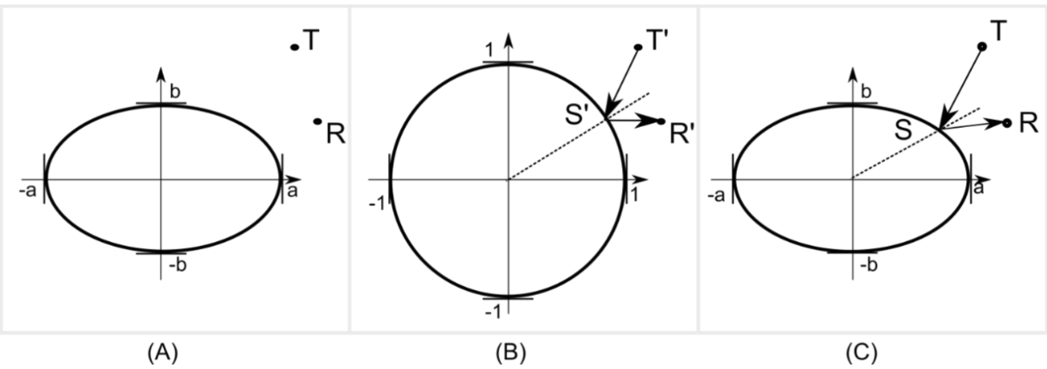

Figure 3.2 Quasi-spherical approximation for determining the specular point location

The method runs as follows:

- Apply a coordinate transformation such that the Earth ellipsoid is scaled in polar and equatorial axes independently down to a sphere of unit radius (Figure 3.2, manipulation from (A) to (B)). The receiver and transmitter locations are equivalently scaled by the same transformation into new (primed) coordinates.

- The specular point is calculated for R’ T’ using the spherical Earth approach.
- The inverse of the coordinate transform is applied to scale back to the original Earth oblate form (C).

Reflection is not invariant under scaling, so the specular point estimate no-longer corresponds to true reflection, but the radial $|\boldsymbol{S}|$ has been corrected back onto the ellipsoidal surface. This correction is important as it mitigates against the great altitude sensitivity of the RST path length. The quasi-spherical algorithm description is as follows:

1. Scale ***R***, ***T*** to a unit sphere using the Earth semi-major (a) and semi-minor (b)

$$\text{Scaling matrix, } \boldsymbol{F} = \begin{bmatrix} \frac{1}{a} & 0 & 0 \\ 0 & \frac{1}{a} & 0 \\ 0 & 0 & \frac{1}{b} \end{bmatrix} \tag{3-1}$$

$$\boldsymbol{R}' = \boldsymbol{FR}\,,\ \boldsymbol{T}' = \boldsymbol{FT} \tag{3-2}$$

2. Determine the location of the specular point on the unit sphere, using spherical approach from [Martin-Neira 1993]. Call the solution, ***S’***
3. Scale the solution back from the unit sphere to the original coordinate system.

$$\boldsymbol{S} = \boldsymbol{F}^{-1}\boldsymbol{S}' \tag{3-3}$$

3.1.3.4 Specular Point Location, Ellipsoid Earth

The L1a processor is able to repeat the specular point location calculated on-board using the ellipsoidal Earth method. Testing is performed on occasion to confirm the onboard calculation matches ground-based calculations. The specular point result is obtained through minimising the path length from transmitter to Earth to receiver [Jales 2015], subject to the solution being on the surface of a WGS-84 reference ellipse.

$$\text{Minimise } \boldsymbol{f}(\boldsymbol{S}) = |\boldsymbol{S} - \boldsymbol{T}| + |\boldsymbol{R} - \boldsymbol{S}| \tag{3-4}$$

$$\text{subject to } \boldsymbol{g}(\boldsymbol{S}) = \frac{S_x^2}{a^2} + \frac{S_y^2}{a^2} + \frac{S_z^2}{b^2} = 1 \tag{3-5}$$

The specular point location $\boldsymbol{S}$, receiver location $\boldsymbol{R}$ and transmitter location is $\boldsymbol{T}$. Here a is the ellipse semi-major axis (equatorial radius) and b is the semi-minor axis (polar radius) of the ellipsoid.

The minimisation is achieved in the processor using the method of successive approximations (MSA, W. B. Gordon 2010). The procedure is as follows:

1. Define mapping function for the bistatic path, where $\boldsymbol{p_0}$ are coordinates that minimise eqn 3.4:

$$\boldsymbol{p_0} = \frac{\boldsymbol{R}|\boldsymbol{T} - \boldsymbol{S}_n| + \boldsymbol{T}|\boldsymbol{R} - \boldsymbol{S}_n|}{|\boldsymbol{R} - \boldsymbol{S}_n| + |\boldsymbol{T} - \boldsymbol{S}_n|} \tag{3-6}$$

2. Define the path length function ($\boldsymbol{f}(\boldsymbol{S_n})$), where $\boldsymbol{I}$ is an identity matrix, $\boldsymbol{S_n}$ is a multivalued function of $\boldsymbol{p_0}$ and A is the symmetric matrix definition of the ellipsoid:

$$\boldsymbol{p_0} \cdot (\boldsymbol{A}\,(\boldsymbol{I} + \boldsymbol{S_n A})^{-2}\,\boldsymbol{p_0}) - \boldsymbol{1} = \boldsymbol{0} \tag{3-7}$$

3. Using Newton’s method, evaluate the path length function and its derivative. Obtain the roots of the function through iteration:

$$\boldsymbol{S_{n+1}} = \boldsymbol{S_n} - \frac{\boldsymbol{f}(\boldsymbol{S_n})}{\boldsymbol{f}'(\boldsymbol{S_n})} \tag{3-8}$$

4. The specular point approximation is obtained as follows once the stopping criteria (**Tol**) has been met, ($\boldsymbol{f}(\boldsymbol{S_n})$ < **Tol**):

$$\boldsymbol{S} = (\boldsymbol{I} + \boldsymbol{S}_{n+1}\boldsymbol{A})^{-1}\,\boldsymbol{p_0} \tag{3-9}$$

The tolerance (Tol) was initially set to 10E-8 metres, but has been reduced to 0.05 metres as very little difference was observed in the results. The limit set at 100 iterations for final calculation.

3.1.3.5 Specular Point Calculation, On-board DEM and Geoid

Table 3-2 SP Calculation Data References

Item	Name	Resln	Coverage	Aggr.	Ref.	Source
Digital Elevation Model	Global Multi-resolution Terrain Elevation Data 2010 GMTED2010 - Elevation	5km	Lat -56 to 84deg	Mean	EGM-96	www.earthenv.org/topography Doc: https://pubs.usgs.gov/of/2011/1073/pdf/of2011-1073.pdf
Geoid Undulation	EGM96 Geoid Model	15 min.	Worldwide	-	WGS-84	https://earth-info.nga.mil/GandG/wgs84/gravitymod/egm96/
Antarctic DEM TBC	Antarctica _Cryosat2 DEM	1km	Antarctic (<-71 deg)	-	WGS-84	www.cpom.ucl.ac.uk/csopr/icesheets2/dems

The specular point is calculated on-board the HydroGNSS instrument to the required accuracy to ensure that the reflected signal appears within the window of the DDM. This information is also available on the ground such that the on-board calculations may be confirmed. First the ellipsoidal Earth function (3.1.3.4) is used to find the reflection point on the WGS-84 ellipsoid, and returns latitude, longitude, and altitude above the reference ellipsoid (*Alt)*.

An on-board Digital Elevation Model, derived from GMTED2010 (Danielson, J.J., and Gesch, D.B., 2011) with a coarse resolution (5 km) is used to calculate the reflection location height over land. Vertical units for the elevation values are integer meters and are referenced to the EGM96 geoid as the vertical datum. The height of the GMTED2010 DEM referenced to the EGM96 geoid surface is found as follows, where (Lat, Lon, Alt) identifies the location of the calculated specular point on the WGS-84 ellipsoid:

$$\boldsymbol{H} = \boldsymbol{F}(\boldsymbol{Lat}, \boldsymbol{Lon}, \boldsymbol{Alt}) \tag{3-10}$$

The function is a look-up table that retrieves the DEM height value at the latitude and longitude from the DEM file at a specified resolution and provides the height above the geoid surface (H). It is important that the DEM file on the ground matches the DEM file on-board the satellite. If the look-up data is not available (for example over ocean or out of range) the original altitude is returned.

In addition to the DEM, the EGM96 Geoid is required to reference the DEM surface to the WGS84 ellipsoid and is also relevant over oceans. This applies over the whole globe, not just the land. This function provides the difference between the ellipsoid and geoid, the geoid undulation (h_g), the value can be positive or negative.

$$\boldsymbol{h_g} = \boldsymbol{F}(\boldsymbol{Lat}, \boldsymbol{Long}, \boldsymbol{Alt}) \tag{3-11}$$

Both heights are used on-board to adjust the DDM to match the location of the specular point over land elevations, h is the height above the ellipsoid:

$$\boldsymbol{h} = \boldsymbol{H} + \boldsymbol{h_g} \tag{3-12}$$

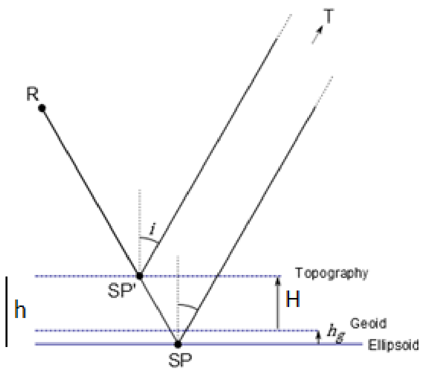

Figure 3.3 Specular point adjustment due to topography (positive Geoid case)

Once the elevation is updated from the DEM and Geoid, the ellipsoid method (FindSpecularPointEllipsoidalEarth: section 3.1.2.4) is repeated with the surface constraint at the new larger ellipsoid (where the larger ellipse axes are defined as *a+h* and *b+h*, therefore WGS-84 eccentricity is not maintained), giving an updated reflection point on the topographic surface referenced to the WGS-84 ellipsoid. The surface at the updated specular point is assumed to be flat, a surface slope is not considered for this calculation.

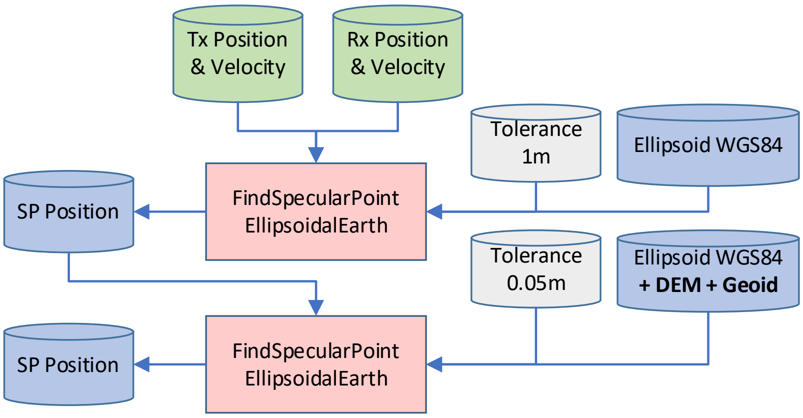

Figure 3.4 Specular Point Update Following Height Adjustment

The on-board DEM function applies a delay and Doppler adjustment in accordance with the predicted location. The delay reduction due to the updated reflection point is approximated by the following equation, however the Level 1a and 1b processors calculate the geometric delay ($dt_{geometric}$) at the updated specular point:

$$d = \frac{2 \cdot h}{\cos(i)} \quad (3\text{-}13)$$

3.1.3.6 Slope Adjustment

For reflections off surfaces with a slope not equal to 0, the specular point will move uphill towards either transmitter or receiver as a function of the surface slope and the elevation angle. The slope adjustment algorithm on the instrument applies a limited compensation for slopes, as subsequently described (and in AD-6). The instrument's algorithm is mirrored in the Level 1A processor for verification purposes and documented here.

3.1.3.6.1 Slope Definition in 1-D

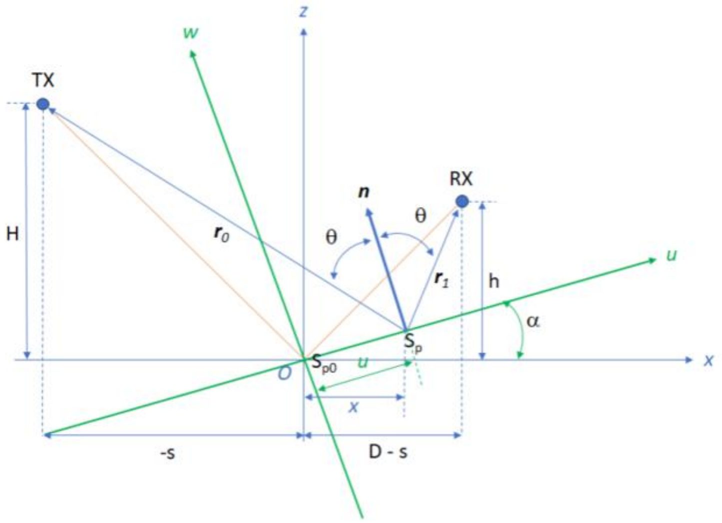

Figure 3.5 Illustration of 1D Slope Definitions

Figure 3.5 shows a slope geometry, making simplifications of system with a flat horizon (x-plane), a transmitter (TX) at height H, a receiver (RX) at height h, and a specular point (S_{p0}) located at the origin (O). A slope is introduced (u-plane) with angle α to the x-plane and which causes the specular point to move to a new location (S_p) that maintains the incident angle equal to the reflected angle (θ).

3.1.3.6.2 2D Slope Angle Calculation

The slope in two dimensions is defined in Figure 3.6. The angle α defines the slope from the x-y plane and the parameter β defines the azimuth angle, or *aspect* of the slope, as anti-clockwise angle from the reflection plane (as viewed from +z direction).

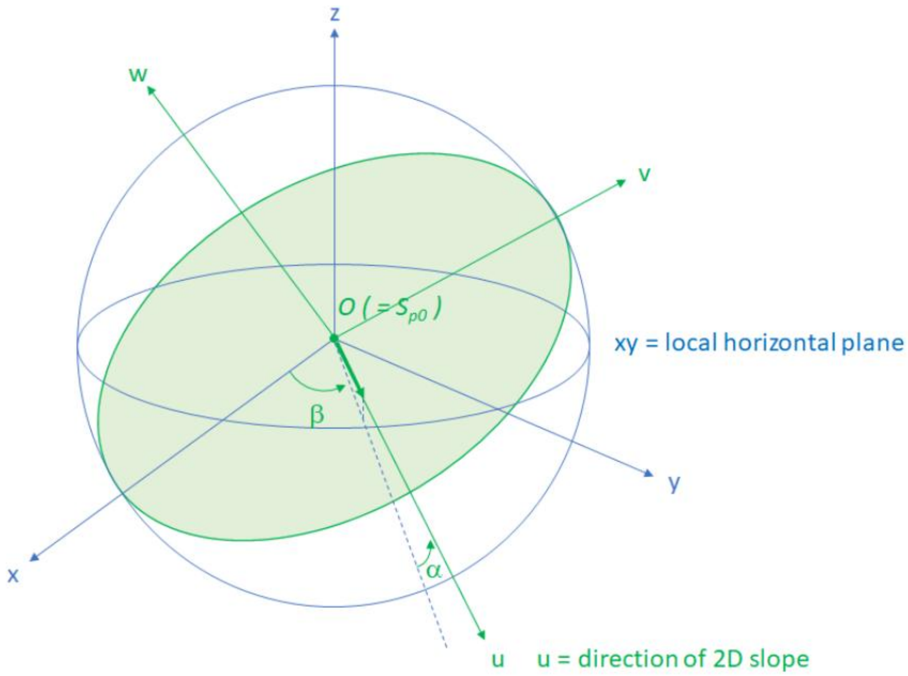

Figure 3.6 Illustration of 2D Slope and O_{uvw} frame definition

The initial specular point SP is found and raised by the DEM and geoid (see section 3.1.3.5). Trial coordinates are determined in a line parallel with the reflection plane, each separated by a specified distance from the next. The height of each point is then found from the DEM, and a line of best fit can be used to determine the slope (α) in 1D. This method is extended to 2D by using another vector normal to the reflection plane, to allow determination of both slope α and azimuth or aspect of slope, β. The two angles are then used to calculate an estimated SP displacement due to the local slope.

The X and Y unit vectors are found parallel to the Earth's surface aligned along the reflection plane, and across the reflection plane respectively as follows:

$$\boldsymbol{Y} = \frac{\boldsymbol{SP}}{|\boldsymbol{SP}|} \times \frac{\boldsymbol{SP-Rx}}{|\boldsymbol{SP-Rx}|}; \qquad \boldsymbol{X} = \frac{\boldsymbol{SP}}{|\boldsymbol{SP}|} \times \boldsymbol{Y} \tag{3-14}$$

Then find points (x_i) along the x-axes at spacing d, and points (y_i) along the y-axis.

$$\boldsymbol{x_i} = \boldsymbol{SP} + \boldsymbol{X}.\left(\boldsymbol{d.i} - \boldsymbol{d}.\frac{\boldsymbol{n}}{2}\right); \ \boldsymbol{y_i} = \boldsymbol{SP} + \boldsymbol{Y}.\left(\boldsymbol{d.i} - \boldsymbol{d}.\frac{\boldsymbol{n}}{2}\right); \ (\boldsymbol{where\ i}\ \{\boldsymbol{0\ to\ n}\},\ \boldsymbol{n\ is\ even}) \tag{3-15}$$

More detailed methods could take increasingly larger samples of the surrounding DEMs (not just in and out of plane) to arrive at an average of the slope and azimuth.

Given the two slopes in x and y respectively, the slope α (between 0 and π) and azimuth β (-π to +π) can be found:

$$\propto = \boldsymbol{atan}\left(\sqrt{\left(\frac{dz}{dx}\right)^2 + \left(\frac{dz}{dy}\right)^2}\right); \quad \boldsymbol{\beta} = \boldsymbol{atan2}\left(\frac{dz/dy}{dz/dx}\right); \tag{3-16}$$

Heights z_i (of points f_i) are found fitted along the y-axis (90°) line using the same fitting process:

$$\text{Out of plane slope estimate } \boldsymbol{dz/dy} = \frac{n\sum_{i=1}^{n} y_i z_i - \sum_{i=1}^{n} y_i \sum_{i=1}^{n} z_i}{n\sum_{i=1}^{n} y_i^2 \left(\sum_{i=1}^{n} y_i\right)^2} \tag{3-17}$$

Two parameters are selectable in this algorithm – the distance between points, *d*, and the number of points, *n*, used in the slope calculation. The processor uses 7km and 4, respectively, it gives a reach of *d*(*n*-1), 28 km for the algorithm. The value of 28 km has been selected as it overlays the resolution upper limit of HydroGNSS, but it is recognised that higher end slope adjustments could move the specular point by more than 50 km, at which point the slope displacement estimate is unlikely to be correct. To avoid excessive slope corrections, a limit of 2.4° is imposed, representing the highest slope expected 95% of the time. For the remaining 5%, the adjustment is limited to 2.4°, so will provide partial correction. Slope correction is not required over the ocean.

3.1.3.6.3 2D Geolocation Adjustment due to Tilted Plane Surface

The vectors towards the transmitters and receivers are represented in the xyz plane as

$$\boldsymbol{H_{xyz}} = \begin{bmatrix} -\boldsymbol{S} \\ \boldsymbol{0} \\ \boldsymbol{H} \end{bmatrix}; \qquad \boldsymbol{h_{xyz}} = \begin{bmatrix} \boldsymbol{D-s} \\ \boldsymbol{0} \\ \boldsymbol{h} \end{bmatrix} \tag{3-18}$$

In tilted uvw frame, these coordinates are rotated by α and β. Abbreviations p_j and q_j are used for convenience.

$$\boldsymbol{H_{uvw}} = \begin{bmatrix} \boldsymbol{p1} \\ \boldsymbol{p2} \\ \boldsymbol{p3} \end{bmatrix} = \begin{bmatrix} -\boldsymbol{s}\cos(\propto)\cos(\boldsymbol{\beta}) + \boldsymbol{H}\sin(\boldsymbol{\alpha}) \\ \boldsymbol{s}\sin(\boldsymbol{\beta}) \\ \boldsymbol{s}\sin(\boldsymbol{\alpha})\cos(\boldsymbol{\beta}) + \boldsymbol{H}\cos(\boldsymbol{\alpha}) \end{bmatrix} \tag{3-19}$$

$$\boldsymbol{h_{uvw}} = \begin{bmatrix} \boldsymbol{q1} \\ \boldsymbol{q2} \\ \boldsymbol{q3} \end{bmatrix} = \begin{bmatrix} (\boldsymbol{D-s})\cos(\propto)\cos(\boldsymbol{\beta}) + \boldsymbol{h}\sin(\boldsymbol{\alpha}) \\ -(\boldsymbol{D-s})\sin(\boldsymbol{\beta}) \\ -(\boldsymbol{D-s})\sin(\boldsymbol{\alpha})\cos(\boldsymbol{\beta}) + \boldsymbol{h}\cos(\boldsymbol{\alpha}) \end{bmatrix} \tag{3-20}$$

the specular point condition of equal angles gives solutions for displacements on *u* and *v* axes as:

$$\frac{p_3}{\sqrt{(p_1-u)^2+(p_2-v)^2+{p_3}^2}} = \frac{q_3}{\sqrt{(q_1-u)^2+(q_2-v)^2+{q_3}^2}} \tag{3-21}$$

This equation can be manipulated, assuming path is on same line from TX to RX, to find equation:

$$(\boldsymbol{u} - \boldsymbol{c_1})^2 + (\boldsymbol{v} - \boldsymbol{c_2})^2 = \frac{{p_3}^2{q_3}^2[(p_1-q_1)^2+(p_2-q_2)^2]}{({p_3}^2-{q_3}^2)^2} \tag{3-22}$$

Where

$$\boldsymbol{c_1} = \frac{{p_3}^2 q_1 - {q_3}^2 p_1}{{p_3}^2 - {q_3}^2}; \quad \boldsymbol{c_2} = \frac{{p_3}^2 q_2 - {q_3}^2 p_2}{{p_3}^2 - {q_3}^2} \tag{3-23}$$

From these equations, u and v, the horizontal displacement in two dimensions can be found from:

$$\boldsymbol{u} = \frac{\boldsymbol{p3q1 \pm q3p1}}{\boldsymbol{p3 \pm q3}} \tag{3-24}$$

$$\boldsymbol{v} = \frac{\boldsymbol{p3q2 \pm q3p2}}{\boldsymbol{p3 \pm q3}} \tag{3-25}$$

The positive roots in this equation apply to the forward scatter location, while negative roots apply to the back-scatter location.

The range error ($\Delta \boldsymbol{l}$) can be found from the predicted range (l_0) and the calculated range including the slope (l_1):

$$\boldsymbol{l_1} = \left[\sqrt{(\boldsymbol{p1}-\boldsymbol{u})^2+(\boldsymbol{p2}-\boldsymbol{v})^2+\boldsymbol{p3}^2}+\sqrt{(\boldsymbol{q1}-\boldsymbol{u})^2+(\boldsymbol{q2}-\boldsymbol{v})^2+\boldsymbol{q3}^2}\right]$$

$$\boldsymbol{l_0} = \left[\sqrt{\boldsymbol{s}^2+\boldsymbol{H}^2}+\sqrt{(\boldsymbol{D}-\boldsymbol{s})^2+\boldsymbol{h}^2}\right]$$

$$\Delta \boldsymbol{l} = \boldsymbol{l_1} - \boldsymbol{l_0} \tag{3-26}$$

Rotation of the horizontal displacement *uvw* to the SP *xyz* frame is as follows:

$$\begin{bmatrix} x \\ y \\ z \end{bmatrix} = \begin{bmatrix} \cos(\propto)\cos(\beta) & -\sin(\beta) & -\sin(\propto)\cos(\beta) \\ \cos(\propto)\sin(\beta) & \cos(\beta) & -\sin(\propto)\sin(\beta) \\ \sin(\propto) & 0 & \cos(\propto) \end{bmatrix} \begin{bmatrix} u \\ v \\ w \end{bmatrix} \tag{3-27}$$

3.1.3.7 Atmospheric Delay Terms

This algorithm has been implemented in Level 1 processor with the intention of matching implementation in instrument. The measured path delay can be affected by both the ionosphere and troposphere. While the tropospheric delay is considered negligible for geolocation of the specular point (centimetres RD-10), the ionospheric path delay is dependent on the total electron content (TEC), the geolocation of the transmitter, receiver and specular point, the time of day and the solar activity. The impact can be in the order of tens on metres, so the path delay through the atmosphere can be estimated to minimise delay error. The path length for the reflectivity calculation is composed of two vectors: from transmitter to the specular point, specular point to receiver.

The ionospheric TEC and delay are predicted using the Neustrelitz Total Electron Content Model (NTCM G, https://www.gsc-europa.eu/) model for L1/E1 and L5/E5A frequencies. The NTCM G algorithm will be implemented onboard and is repeated at L1a:

- Galileo navigation data provides three ionospheric model parameters required for input into NTCM (broadcast coefficients ai0, ai1 and ai2), which are used to compute a single frequency correction.
- At each specular point the geometric range is calculated for the two path lengths including DEM and geoid: from transmitter to specular points, from specular point to receiver.
- Run NTCM G module two times, once for each path.
- Compute the actual total time delay at each specular point (dt_{iono}).

$$dt_{iono} = \boldsymbol{F}(\text{ai0}, \text{ai1}, \text{ai2}, \text{time}, \text{Tx Position}, \text{SP Position}) + \boldsymbol{F}(\text{ai0}, \text{ai1}, \text{ai2}, \text{time}, \text{SP Position}, \text{Rx Position}) \tag{3-28}$$

3.1.3.8 Overall Geolocation Delay

The instrument calculates the specular point location onboard and allocates delay and Doppler value to the coherent channel and to the reference point of the DDM (offset towards the lower delay edge of DDM). The resultant onboard delay (referenced to direct signal reception) is made available such than the geolocation calculation is able to be verified on the ground, although this calculation is not performed routinely in L1 processor or result provided in metadata.

$$dt_{total} = dt_{geometric} + dt_{iono} \tag{3-29}$$

3.2 L1A TO L1B PRODUCTS (L1BOP)

The SSTL level 1b processor (L1BOP) generates metadata including the GNSS receiver radiometric corrections, based on the receiver antenna pattern and the nadir black body measurements. The level 1b metadata also calculates the reflection coefficient and bi-static scattering coefficient (or sigma-0) from the DDMs.

The L1b metadata shall also include collated auxiliary data, gathered from other sources than the platform and payload data.

Table 3-3 L1a to L1b processing

Type	Data	Format	Note
Inputs:	L1a Metadata (including ancillary data)	*.netCDF	See HydroGNSS PDGS Algorithm ICD [AD-1]
	L1a DDM/Coherent Measurements	*.netCDF, 1Hz DDM	
	Blackbody and Direct L1a files	*.netCDF	
Auxiliary	High Resolution Antenna gain map for looking up the gain of the nadir and zenith antennas	*.xagm	Antenna pattern derived pre-launch or from L1BOP-DX-L Both frequency bands, both polarisations
Auxiliary	L1BOP-PX Flags	*.netCDF	Status of the antenna patterns used in the processing, derived from ocean calibration processor (L1 LHCP, possibly also L5 LHCP, TBD)
Auxiliary	GPS/Galileo transmitter satellite ephemerides from RINEX files, giving the position and velocity of the transmitters	RINEX Navigation Data Files	
Auxiliary	GPS/Galileo transmitter SVN to PRN mapping table	*.I14	Example provided here: ftp://ftp.aiub.unibe.ch/BSWUSER52/GEN/SATELLITE.I14
Auxiliary	GPS/Galileo transmitter antenna gain patterns and transmit powers	*.I14	Obtained from published data or generated from L1BOP-DX-L
Auxiliary	Earth topographic map (DEM) Geoid	*.TIFF	See Table 3-2.
Auxiliary	Land Cover map	netCDF value per SP	https://land.copernicus.eu/global/content/annual-100m-global-land-cover-maps-available
Auxiliary	Snow/Ice Data (Being implemented)	netCDF value per SP	https://nsidc.org/data/explore-data
Outputs:	L1b core metadata (including): Specular Point (Angles, Height, X, Y, X, Lat, Lon) Calibration Data Received Power Metrics Transmit Power Metrics Flags	*.netCDF, 1Hz	See HydroGNSS PDGS Algorithm ICD [AD-1]

3.2.1 Theoretical Description

The following sections provide an outline of the L1A to L1B processing pipeline.

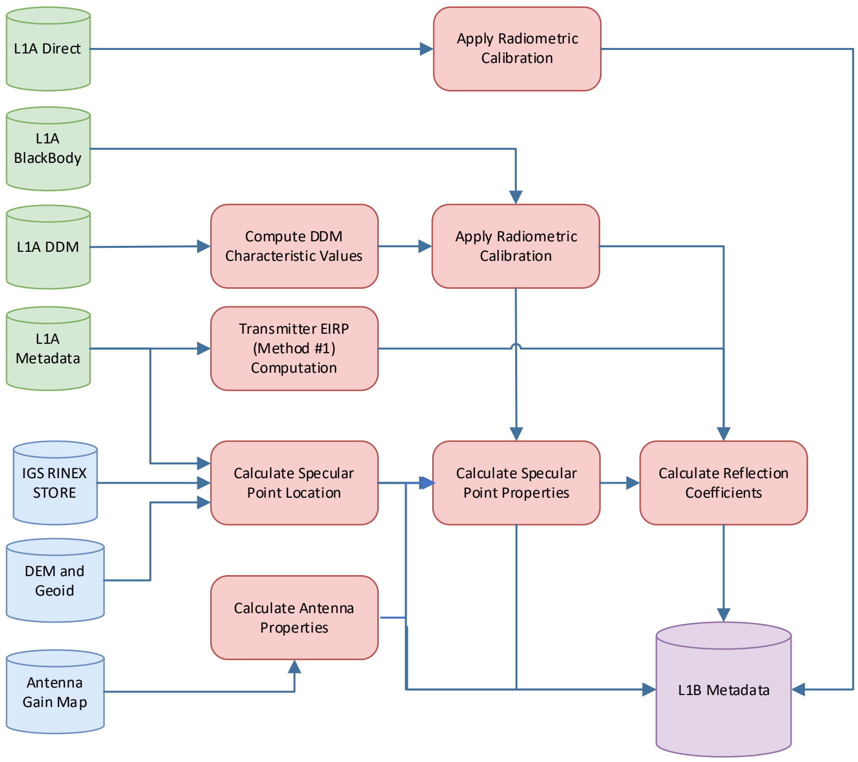

Figure 3.7 L1b Processing

3.2.2 Geometry and Geolocation

As per Section 3.1.3, the instrument calculates the location of the specular point on-board to sufficient accuracy to place the signal within the Delay Doppler Map and to place the coherent channel close to the nominal reflection point. The geometric metadata from Level 1A are used, and the transmit, receiver orbit and specular point are not currently recalculated in Level 1B processor. No added atmospheric terms are applied. A bounding box, however, is applied at Level 1B.

3.2.2.1 Bounding Box Implementation

A bounding box, is applied at Level 1B to allow a constraint of measurements to a location near the geolocated reflection point, allowing better registration of higher resolution measurements. A subset of pixels from the DDM is selected from which the strongest peak is selected. [NB L1OP1.0.8 release and earlier versions used maximum peak within whole DDM].

A configurable bounding box as a subset within the DDM is used to find the peak pixel value. The delay dimension of the bounding box is given in microseconds (nominally 5360) while the doppler dimension is given in Hz (nominally 2500). This is divided by the resolution, delay and doppler, of the DDM, to give the box size in number of delay pixels x number of doppler pixels. In the doppler dimension the box is split evenly to either side of the tracking point. Whereas in the delay dimension, the box is stipulated to be one tenth above the tracking point, or a single row whichever is the larger, and nine tenths below the tracking point. The tracking point is determined on-board and is expected to be one quarter below the top of DDM. The maximum pixel value within this box is used in section 3.2.4.3 to calculate the peak power.

A further parameter is output from the L1 processor that gives the reflectivity from the peak within the whole unbounded DDM and gives the distance of peak from geolocated point (*ReflectionCoefficientUnbounded)*. This is available for research, but not expected to be used by the Level 2 processors. There is also an output parameter produced by the L1B_CX that gives distance of signal peak from geolocated point (DDMPeakOffsetDistance), see RD-4.

The application of the bounding box is as follows for each signal type:

- Define a square of a configurable number of pixels around the pixel at the centre of the DDM (defined delay and Doppler lines plus offset from geolocated point)
- Locate the signal maximum within this bounding box.
- Calculate reflectivities based on peak within box.

- This bounding box is configurable to different sizes to contain the measurements to within a defined uncertainty from the geolocated point, see Table 3-4 (from AD-6).

Table 3-4 Provisional Bounding Areas for Resolution

Target Resolution	L1 Delay Lines after 0	Doppler Lines	L1 - Estimated Distance / Uncertainty	L5 Delay Lines	L5 - Estimated Distance / Uncertainty
25 km x 25 km	22	5	18 km / 36 km	~50 (DDM limited)	13 km / 26 km
12 km x 12 km	11	3	9 km / 18km	33	9 km / 18km
9 km x 9 km	7	1	6 km / 12 km	21	6 km / 12 km
Coherent Channel	1 (+1 either side)	1	0.8 km / 1.6 km (2.4 km / 4.8 km)	1	0.8 km / 1.6 km
Entire DDM	52	20	43 km / 86 km	52	14 km / 28 km

3.2.3 Antenna Gain and Attitude

The antenna gain and attitude for both the transmitter and receiver are important for correcting signal power measurements. The antenna gains at each measurement point are determined as follows, for each of the three antennas: transmitter, receive zenith and receive nadir.

- Antenna map for each antenna is available containing an array of antenna gain in dB against azimuth and elevation.
- Lookup the gain in either published or learnt Tx antenna patterns based on the azimuth and elevation of each measurement.
- Linear interpolation between the grid points is performed to obtain the antenna gain for each measurement.
- The nadir receive antenna patterns also contain cross-polar terms as a function of angle. These are available from ground-based testing, but the terms are not currently used operationally in the Level 1 processor. Tests with the End-to-end simulator showed that the ANN Level 2 processors were capable of being trained using uncorrected LHCP and RHCP measurements to benefit from the two polarised measurements.

3.2.3.1 Antenna Gain at the Specular Point (AGSP)

Determination of the receive antenna reference frame is achieved following the description in appendix (A.1.3). The antenna gain related to a particular vector can be found using the ancillary Antenna Gain Map (AGM) look-up tables. The tables are indexed into using the antenna vector’s azimuth and elevation. A full description of the HydroGNSS reference frame is captured in RD-14.

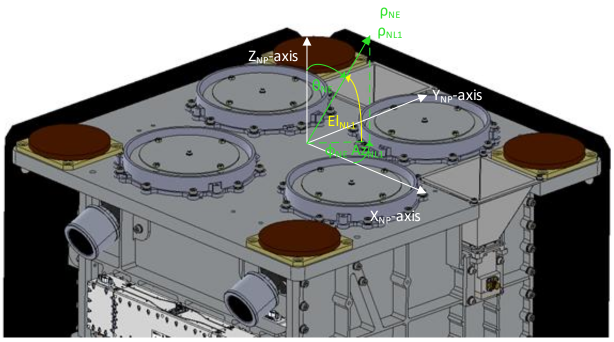

Figure 3.8 Nadir Antenna Diagram (RD-14)

The centre of the nadir antenna array is the origin for the GNSS reflectometry signal measurements, this frame is aligned to the electrical boresight of payload antenna. The positive direction is away from the nadir antenna, the negative direction is the antenna boresight for HydroGNSS zenith antenna.

Elevation is the angle between the X_{NP}/Y_{NP} (nadir payload reference) plane and the unit vector (P_{NL1}), the positive sense is towards the $+Z_{NP}$ axis. EL_{NL1}:

$$El_{NL1} = 90 - \theta_{NE} \quad (3\text{-}30)$$

Azimuth is the smallest angle subtended between the projection of the P_{NL1} onto the X_{NP}/Y_{NP} (nadir payload reference) plane and the X_{NP}-axis, the positive sense is from the X_{NP} towards the Y_{NP} axis. Az_{NL1}:

$$Az = \begin{cases} \phi_{NE} & if\ \phi_{NE} \le +180 \\ \phi_{NE} - 360 & if\ \phi_{NE} \ge +180 \end{cases} \tag{3-31}$$

3.2.3.2 Transmit Antenna Patterns

GNSS published antenna patterns are available for GPS Block IIR, IIR-M, IIF and III. Directivity rather than gain of the antennas is provided in many of the published patterns, a published gain correction factor (GCF) is available and can be applied as required to convert directivity to gain. In Level 1b this conversion is not required as the published or learnt power used in the EIRP algorithm includes the GCF, to effectively give the transmit power. The use of direct signals for CM#3 and antenna pattern learning is described in L1BOP_DX, Section 3.3.

3.2.3.3 GNSS Transmitter Attitude

It is assumed operational GNSS transmitters always point accurately towards the Earth (roll and pitch are ~0°), while the yaw varies systematically to maintain simultaneous Earth-pointing of payload and sun pointing of panels. If yaw is ignored, asymmetries in the transmit antenna patterns can cause small errors in transmit power estimation. Calculation of the GNSS Transmit attitude yaw angle is used for the EIRP calibration method#1 and is made available for use by CM#2 and CM#3. For CM#1 the yaw allows for estimation of the Tx piercing angle towards the SP. Similarly for CM#3, the EIRP knowledge is required pointing towards the HydroGNSS antenna, although an estimation of CM#3 can be made without the yaw angle, by using the average gain at each elevation angle and the ZSR method (see section 3.3.3).

3.2.3.3.1 Nominal Yaw Steering

The following concept is utilised for both GPS and Galileo constellations considering differences in the reference frames. The base algorithm is extracted from the European GNSS Service Centre (www.gsc-europa.eu/support-to-developers/galileo-satellite-metadata).

$$\psi_0 = \text{atan2}[\, \vec{s}(t) \cdot \vec{n}(t), \vec{s}(t) \cdot \vec{r}(t) \times \vec{n}(t)\,] \tag{3-32}$$

Parameters are defined as follows:

- ψ_0, the nominal yaw angle (0 to 360 degrees)
- t, the on-board time
- $\vec{r}(t)$, normalised satellite position vector, ECI frame at J2000 epoch
- $\vec{n}(t)$, normalised orbit vector, ECI frame at J2000 epoch
- $\vec{s}(t)$, normalised Sun position vector, ECI frame at J2000 epoch

The local antenna frame assumed is a generic frame where -X points to nadir and +Z points as close as possible to the Sun (within the yaw degree of freedom). The satellite reference frames differ between manufacturer (constellation and block). In the case where -Z is sunlit both components of the atan2 function change sign.

3.2.3.3.2 Modified Yaw Steering

The L1b processor does not model the transmitter yaw behaviour through non nominal steering conditions. The nominal yaw is reported at L1b for all circumstances, and then a flag is raised (3.2.8.7) where a manoeuvre or shadow crossing is predicted (during low sun-satellite collinearity periods). Where the non-nominal yaw value is provided the Tx antenna piercing angle knowledge is degraded, specifically, the antenna azimuth angle. This introduces uncertainty in the Tx antenna gain but, the error will be less than the total azimuthal variation in the antenna pattern, since the elevation remains known, and the real yaw angle is well within 180 degrees of the provided nominal yaw angle.

The modified yaw steering regime is used where the following conditions are met:

- The sun elevation angle β, between orbit plane and sun vector, is smaller than 4.1 degrees.
- The collinearity angle ε, the satellite and sun position vector angle, is smaller than 10 degrees.

Beta angle is calculated as:

$$\beta = 90° - acos(\, \vec{s}(t) \cdot \vec{n}(t)) \tag{3-33}$$

Collinearity angle is calculated as:

$$\vec{x} = \vec{n} \times \vec{s} \tag{3-34}$$

$$\vec{y} = \vec{n} \times \vec{x} \tag{3-35}$$

$$\varepsilon = \begin{cases} \mathrm{acos}(\vec{r} \cdot \vec{y}) & if\ \mathrm{acos}(\vec{r} \cdot \vec{y}) \le 90° \\ 180° - \mathrm{acos}(\vec{r} \cdot \vec{y}) & if\ \mathrm{acos}(\vec{r} \cdot \vec{y}) > 90° \end{cases} \tag{3-36}$$

3.2.4 Received Power Metrics

The radiometric corrections follow the path laid by TDS-1 (RD-15) to find the received power at the reflection point. Correction is required for reflection (nadir) and direct (zenith) paths (Figure 3.11). The result of the calibration is to determine the metric of power incident at the receiver antenna or the reference point (LNA input). Different metrics have been developed in the past, including peak power, integrated power (in delay and Doppler), leading edge-slope, and trailing-edge slope. The primary metric used for TDS is the peak power within the DDM. However, the peak in the DDM may originate from terrain features external to the calibrated specular point (topography or water bodies). For HydroGNSS a bounded peak search (see section 3.2.2.1) is performed within an optimal number of pixels around the nominal specular point (the DDM crosshairs), however the following calibration process is the same whether the peak search includes the entire DDM or a portion of it as specified in a geolocated bounding box.

The principles of the radiometric calibration are:

- The RF front-ends are always set to a known gain such that the absolute noise and hence reflected signal can be separated from SNR and measured. The low level front-end Automatic Gain Control (AGC) is not used, but a software-based AGC (swAGC) implemented within the signal processing of the instrument allows the RF gain to be adjusted optimally and reported to the user. See Section 3.2.4.6.
- A temperature reading from the LNA is collected and used to estimate the LNA Noise Figure based on pre-launch measurements. See 3.2.4.6.
- The maximum signal in the DDM is measured, bounded by geolocation, as applicable.
- The noise of the DDM is measured (away from the signal). See 3.2.4.3.
- The blackbody load is switched at a specified cadence (nominally 5 seconds every 10 minutes for nadir, 100 minutes for zenith, switched in for 5 seconds), and a noise reading is taken from the nearest blackbody collection. With a known noise figure, a known temperature, and a measured noise, this allows the instrument gain to be estimated and extrapolated to the time of a measurement. See 3.2.4.6.
- If there is a differential between antenna noise and switched blackbody noise, the swAGC will adjust, which could take 2 or 3 seconds to achieve optimal gain. The gain control and %mag are reported every second so this settling can be monitored.
- The antenna noise can be measured over an external target, this can be used to validate the effectiveness of the blackbody correction scheme.

The payload diagram (Figure 3.11) shows the reference points and terms used in the radiometric corrections of each path, where the internal temperature parameter names (captured by the ICD, AD-1) are mapped to each path as follows:

- Nadir LNA0 = `InternalTemperatures0`
- Nadir LNA2 = `InternalTemperatures1`
- Zenith LNA2 = `InternalTemperatures2`
- Nadir FE0 = `InternalTemperatures3`
- Zenith FE1 = `InternalTemperatures4`

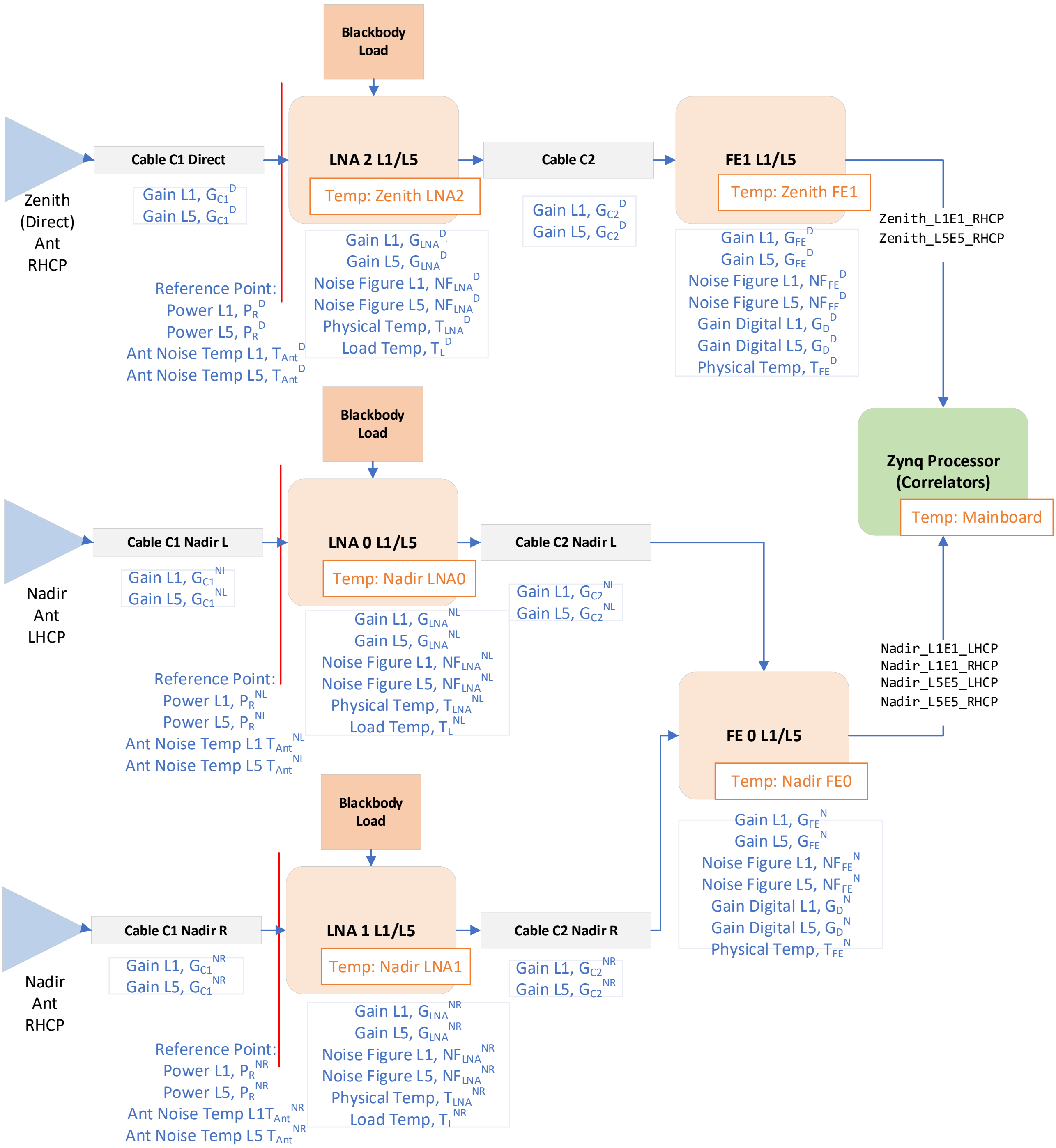

Figure 3.9 Forward model of the Received Signal Power

The sequence of steps from raw data to calibrated power and reflectivity is outlined below and each step is detailed in the following sub-sections:

- Calculate noise temperatures from LNA physical temperature and prelaunch constants (section 3.2.4.4).
- Calculate gain temperature compensation from blackbody and LNA physical temperature (section 3.2.4.6).
- Calculate system gain from black body noise count and noise temperatures (3.2.4.4).
- Calculate mean noise from DDM (section 3.2.4.1).
- Calculate the bounded peak power around the calibrated specular point, the mean noise and system gain (section 3.2.4.3).
- Extend from the reference point to the receiver nadir antenna (section 3.2.4.7) including the cable C1.
- Calculate reflection coefficients (section 3.2.6), incorporating antenna gains and path losses.

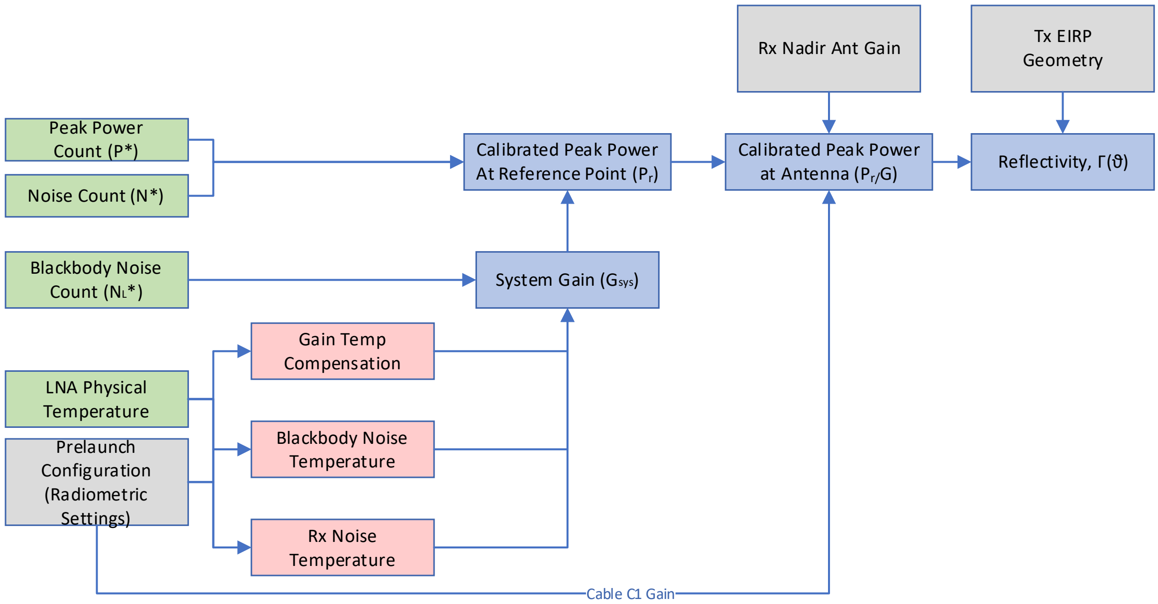

Figure 3.10 Peak Power Calibration (including reflectivity)

3.2.4.1 Sampling and Implementation Loss

Measurements made from the DDMs at the signal P*, and at noise floor N* both are affected by the finite sampling rate, quantisation into 2 bits, and filtering that occurs before sampling and filtering as part of the correlation process after sampling. From literature e.g. [HEG11], filtered two-bit sampling implementation signal loss $L_s$of around 1.5 dB is expected. The effects of sampling on noise measurements $L_n$are different to L_s due to the spread over bandwidth and quantisation effects manifesting as noise. But the reference noise is significantly amplified by the LNA, so could be considered as behaving like a signal, with similar losses. The ratio of losses between sampling signals and sampling noise L_s/L_n defines the change in the signal to noise during the sampling process.

The $L_s$term can cause a change in the System Gain, but if L_s and L_n are assumed equal (ratio of 1) they indirectly cancel out from analysis in determining reflected power. From tests using calibrated signals into the instrument, this ratio has been estimated as 1.3 for L1 $(\frac{L_s}{L_n} = 1.3 \; or \; 1{,}1 \; dB)$ but may be investigated further during the mission. NB -to remain compatible with TDS-1 data processing, this ratio may be initially set to 1, such that SNRs values match those on previous missions.

3.2.4.2 Noise Estimation

The estimate of the noise power in the DDMs (N^*) is determined using a set of pixels known to be separated from the reflected signal. The average power is obtained for the DDM pixels corresponding to a path delay less than for the specular path. Over the ocean surface, there are no physical reflectors above the surface and so this area of pixels contains just the thermal noise and any interference. Figure 3.11 (L) shows a DDM over the ocean. It is beneficial to choose as many noise pixels as possible to reduce the variance of the noise estimate.

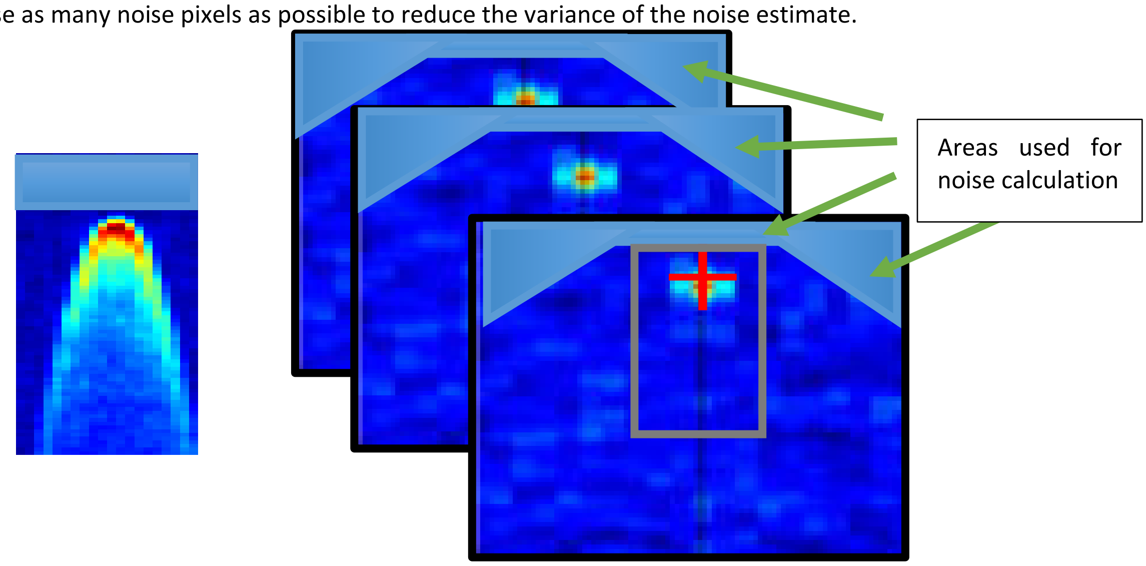

Figure 3.11 (Left) Typical DDMs processed over the ocean (grey box corresponds to the 'Noise Box') (Right) Using box, corners, and multiple DDMs for noise determination.

Over the land, however, at times there may be reflections from higher topographies, so additional margin may be required. On TDS-1, the reflection over land moved up the DDM as the elevation increased, so the noise box had to be reduced in size using a topographic map in MERRByS ground processing. On HydroGNSS, the DDM is adjusted according to the on-board DEM, so the noise box does not need resizing.

For HydroGNSS, the size of the DDM is reduced (compared to TDS-1) this leaves fewer rows available for the noise box. Instead, the noise pixels are selected in the following way:

- All the pixels from the top delay row and subsequent delay rows down to a configurable number of rows (nominally five) above the tracking point.
- All the pixels from the top corners of the DDM. The corners are defined by a single configurable value (nominally six) used for the delay and doppler dimensions then all the pixels inside the triangle described by these points are selected.
- The same pixels are selected from a configurable number (nominally five) of DDMs before and after the current DDM. At the start or end of a track where there are not enough DDMs before or after the current DDM respectively then fewer DDM's are used.

The measured noise at time of signal is

$$N^* = kB(T_{ant} + T_{rx})G_{sys}/L_n \tag{3-37}$$

Where T_{ant} is the antenna noise, T_{rx} is the receiver noise temperature, G_{sys} is the system gain from reference point to signal processed results, L_n is estimated sampling loss for noise. The k is Boltzmann's constant. Bandwidth at the RF front-end is approximately 25 MHz, but is later filtered during the digital correlation process, which at 4 millisecond integration gives 250 Hz.

While the blackbody is switched in, there are no signals so all the pixels in the DDM can be used to determine the average noise. Assuming the sampling loss for the noise remains the same, the noise at time of blackbody load is:

$$N_L^* = kB(T_L + T_{rx})G_{sys}/L_n \tag{3-38}$$

These equations initially assume the system gain and receiver noise temperature remain the same for both measurements, but corrections can be made if this is not the case (discussed below).

3.2.4.3 Peak power

Following the terminology in TDS-1 (RD-3), the <DDMOutputNumericalScaling> L1b field contains the correlation count of the DDM peak power including noise in each DDM; it is the maximum DDM pixel value before scaling to 65535 for the 16-bit storage range.
This <DDMOutputNumericalScaling> parameter is required to remove the scaling applied to each DDM pixel.

For earlier Level 1 processors (L1OP v1.0.8 as used with E2ES), <DDMSNRAtPeakSingleDDM> contains the peak power out of the whole DDM used for the specular point measurement (P^*). But for later processors, <DDMSNRAtPeakSingleDDM> contains the result from a separate peak search applied to the defined bounded box. P^* and N^* can then be correctly scaled. It is assumed that noise is additive to the signal, therefore P^* measurement contains the noise as well as signal, and the average noise needs to be subtracted to recover the signal power alone. Accounting for this, the unbiased signal to noise ratio (SNR) in dB can be determined.

$$SNR = 10\log_{10}\left(\frac{P^*L_s - N^*L_n}{N^*L_n}\right) \quad \text{[in dB]} \tag{3-39}$$

If losses L_s and L_n are assumed equal these terms cancel out, and the uncompensated SNR can be found – this is the version of the SNR mostly used for TDS-1 and other analyses. The scaling of SNR_u is linked to the instrument and is not affected by assumptions made about the noise loss ratio.

$$SNR_u = 10\log_{10}\left(\frac{P^*}{N^*} - 1\right) \quad \text{[in dB]} \tag{3-40}$$

The P^* measurement contains signal added onto the noise floor, and assumed L_s term applies.

$$P^* = \left(P_r^S + kB(T_{ant} + T_{rx})\right)G_{sys}/L_s \tag{3-41}$$

To determine the power received at the input to the LNA reference point (P_r^S), radiometric correction of the Signal Minus Noise digital measure is used, this accounts for the analogue (LNA, Cable 2, FE) and digital (ADC conversion) gains.

$$P_r^S = \frac{(P^* L_s - N^* L_n)}{G_{Sys}} \quad (3\text{-}42)$$

3.2.4.4 System Gain and Noise Figure

The total system gain at the nadir (G_{Sys}) includes the analogue gain and the digital gain due to conversion from ADC counts to correlator processing.

$$G_{sys} = G_{LNA} G_{C2} G_{FE} G_D \quad (3\text{-}43)$$

The system gain can vary due to changes in the physical temperature of the LNA and receiver, and if the IF Gain settings are changed. When using the swAGC mode, the IF settings are adjusted automatically to ensure the amplitude matches the optimal digital sampling amplitude (i.e. %mag ~=33%). If a strong signal is received through the antenna (i.e. high antenna temperature value), the IF gain settings, and hence system gain will be reduced to maintain the correct %mag.

The gain is measured using the LNA's internal blackbody load, or using an external reference, for example in the Antarctic. The gain in the system can be obtained from rearranging the noise measurement taken while the blackbody reference is switched in, N_L^*:

$$G_{sys} = \frac{N_L^* L_n}{kB(T_L + T_{rx})} \quad (3\text{-}44)$$

T_L and T_{rx} define the blackbody load and receiver noise temperature respectively. The receiver figure is calculated from the measured physical temperature of the components, and radiometric data obtained on ground before flight. The receiver noise temperature can be determined using Friis cascade equation.

$$\mathrm{T_{rx}} = \mathrm{T_{LNA}} + \frac{\mathrm{T_{C2}}}{\mathrm{G_{LNA}}} + \frac{\mathrm{T_{FE}}}{\mathrm{G_{LNA}G_{C2}}} \quad (3\text{-}45)$$

Where T_{LNA} is the effective noise temperature of the LNA. T_{FE} is the front-end effective noise temperature (of less significance due to due to G_{LNA} term as divider). Given a Noise Figure in dB, and temperature of a device in Kelvin (T_0), the effective noise temperature can be found by

$$\mathrm{T_{LNA}} = \mathrm{T_0}(10^{(\mathrm{NF_{LNA}(dB)}/10)}\text{-}1) \quad (3\text{-}46)$$

Pre-launch calibration information allows an estimate of noise figure and gain for the LNAs at a specified temperature (x in °C), allowing estimates at the time of the BB, and the time of the reflection measurement.

$$NF_{LNA} = \mathrm{m}_{LNA}\mathrm{x} + \mathrm{c}_{LNA} \text{ [in dB]} \quad (3\text{-}47)$$

Likewise the change in gain of the LNA can be estimated.

$$G_{LNA} = \mathrm{m}_{gLNA}\mathrm{x} + \mathrm{c}_{gLNA} \text{ [in dB]} \quad (3\text{-}48)$$

A system gain measurement and radiometric parameters are provided by the processor for each front-end blackbody measurement (for each path in Figure 3.9). Typical values are shown in Table 3-5.

Table 3-5 Representative values for LNAs NF and Gain

Freq Band	m_{LNA}	c_{LNA}	m_{gLNA}	c_{gLNA}
L1	0.00449	0.903	-0.0230	30.87
L5	0.00451	0.784	-0.0297	30.76

3.2.4.5 Compensation for AGC changes

To allow recovery of the gain from the instrument's RF section (hence allowing measurement of received power), the gain of the system must either be fixed or, if operated under Automatic Gain Control (AGC), the gain setting must be known. The SGR-ReSI-Z can be operated in a) hardware AGC mode, b) fixed gain mode, or c) swAGC mode, but the latter is the baseline mode.

The swAGC is a software-based Automatic Gain Control function (Figure 3.12) and when enabled automatically adjusts the gain each second and reports the gain settings back to ensure that the output remains near the 2-bit optimal sampling region, where 33% of the measurements are flagged as higher magnitude. Every second, for each RF channel, the swAGC operates. The %mag is determined by counting higher magnitude bits read at sampling rate from the last 100 ms integration, and divided by the total number of samples. If %mag is more than 10% (adjustable threshold) away from optimum, the fine IF gain step adjusted by one step (approx. 0.5 dB gain), either up or down depending on the polarity of the offset. If the %mag is larger than a certain threshold, the coarse gain is switched (approx. 3 dB gain), and fine gain is set to mid-range. The coarse gain is also adjusted if the fine gain reaches a limit.

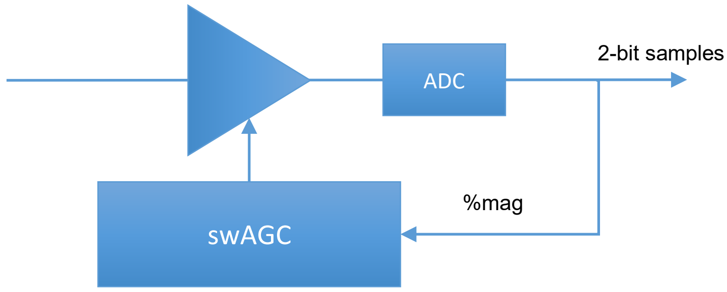

Figure 3.12 Software Automatic Gain Control (swAGC) Schematic

The programmable gain of the front-end can be modelled (in dB) as a function of 3 registers:

$$G_{AGC(T0)} = (12+0.97*\text{RF Gain setting}) + \text{LookupIF(coarse IF)} + \text{LookupIF(fine IF)} \quad [\text{dB}] \qquad (3\text{-}49)$$

The *RF gain setting* is by default set at maximum 0xF which gives an RF gain value of (12+14.55), i.e. 26.55 dB.

The *IF coarse* and *IF fine* gain settings translate into additional gain according to look up values in Table 3-6:

Table 3-6 Front-end Gain Determination at ambient (italic text from datasheet, otherwise interpolated)

Coarse IF Value (bin)	Decimal	Gain (dB)		Fine IF Value (bin)	Decimal	Gain (dB)
"00000"	*0*	*-0.5 dB*				
	1	3.2				
	2	6.8				
"00011"	*3*	*10.5 dB*				
	4	13.6				
	5	16.6				
	6	19.7				
"00111"	*7*	*22.7 dB*		*"00111"*	*7*	*-0.35 dB*
	8	25.6		*"01000"*	*8*	*-0.30 dB*
	9	28.6		*"01001"*	*9*	*-0.10 dB*
"01010"	*10*	*31.5 dB*		*"01010"*	*10*	*0.30 dB*
	11	33.9		*"01011"*	*11*	*0.90 dB*
	12	36.3		*"01100"*	*12*	*1.70 dB*
	13	38.6		*"01101"*	*13*	*2.40 dB*
"01110"	*14*	*41.0 dB*		*"01110"*	*14*	*3.00 dB*
	15	44.2		*"01111"*	*15*	*3.40 dB*
	16	47.5		*"10000"*	*16*	*3.80 dB*
"10001"	*17*	*50.7 dB*		*"10001"*	*17*	*4.10 dB*
	18	53.3		*"10010"*	*18*	*4.40 dB*
	19	55.9		*"10011"*	*19*	*4.55 dB*
	20	58.4		*"10100"*	*20*	*4.70 dB*
"10101"	*21*	*61.0 dB*		*"10101"*	*21*	*4.80 dB*
	22	62.3		*"10110"*	*22*	*4.90 dB*
"10111"	*23*	*63.5 dB*		*"10111"*	*23*	*5.00 dB*
				"11000"	*24*	*5.05 dB*
				"11001"	*25*	*5.10 dB*

This look-up table is defined at room temperature, 25°C. The equation can be modified to approximately account for temperature variations.

$$G_{AGC(T)} = G_{AGC(T0)} + 2.5 - 0.1 * \text{F/E Temperature (°C)} \quad [\text{dB}] \qquad (3\text{-}50)$$

This equation allows the modelling of absolute gain, but more importantly the delta-gain between settings, which can be used to correct blackbody-calibrated measurements which may have been taken with a different gain setting.

$$G_{deltaAGC} = G_{AGC,R}/G_{AGC,L} \qquad (3\text{-}51)$$

where $G_{AGC,R}$ is AGC gain setting at time of reflection measurement and $G_{AGC,L}$ at time of blackbody load measurement. This gain delta term is applied to the system gain in the next section. Measurement of fine IF gain compared to datasheet values (see Figure 3.14) shows that the results are close, and the delta-gain is even closer with fine IF maintained between the range of between 10 and 18 dB.

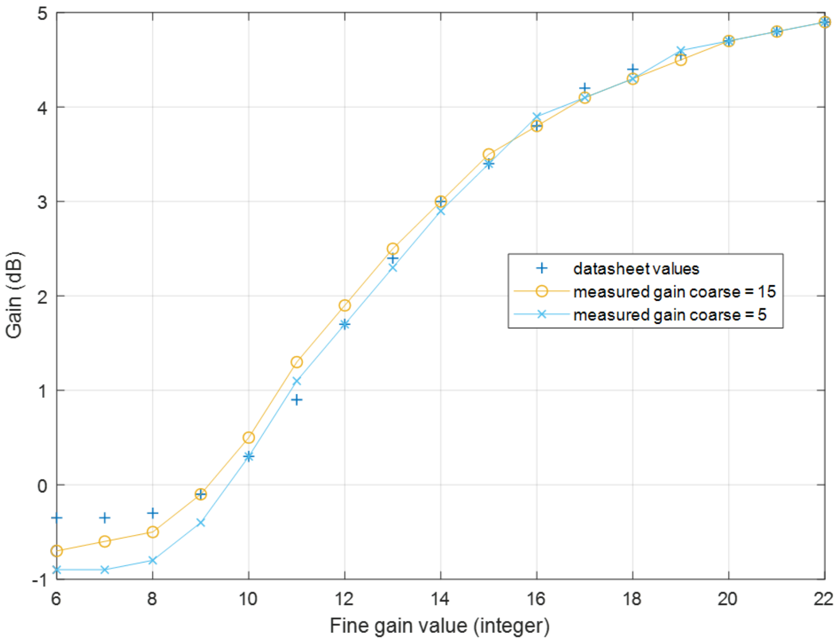

Figure 3.13 Behaviour of front-end gain with fine and coarse gain settings, measured vs datasheet.

3.2.4.6 Delta-Gain Changes

The blackbody measurement from which system gain is determined takes place at a different time to the measurement of signals. The temperature changes in the LNA may mean that the noise figure and gain have changed. $G_{deltaLNA}$ is an additional term that accounts for change in LNA Gain due to change in temperature since the estimation of G_{LNA} from the blackbody measurement and uses measured temperature difference and known LNA gain gradient.

$$G_{deltaTLNA} = G_{LNA,R}/G_{LNA,L} \tag{3-52}$$

Where $G_{LNA,R}$ and $G_{LNA,L}$ are gains determined at the time of reflection measurement and blackbody loads accounting for different LNA temperatures.

An updated estimate of gain is then found by:

$$\hat{G}_{sys} = G_{sys}\,\Delta G = G_{sys}\,G_{deltaTLNA}G_{deltaAGC} \tag{3-53}$$

And the adjusted reflectometry power (as per Equation (3-42) can be determined by

$$P_r^S = \frac{(P^*L_S - N^*L_n)}{\hat{G}_{sys}} \tag{3-54}$$

3.2.4.7 Signal at antenna connection

The signal power can be found at the connection to the antenna port by accounting for gain (inverse of loss) of Cable 1.

$$P_r = P_r^S/G_{c1} \tag{3-55}$$

3.2.4.8 Antenna Noise Temperature

The antenna noise power is the overall power received by the nadir antenna and can be a useful metric to observe variations in background noise, separated from the reflected signals. The antenna noise power can be found from dividing the noise power measurements from the antenna by those from the blackbody (and assuming sampling noise losses cancel)

$$\frac{N^*}{N_L^*} = \frac{kB(T_{ant}+T_{rx,R})(G_{sys}\Delta G)}{kB(T_L+T_{rx,L})G_{sys}} \tag{3-56}$$

where $T_{rx,L}$ and $T_{rx,R}$ are the noise temperatures at time of load and reflection measurements. Rearranging for T_{ant}, this becomes,

$$T_{ant} = \frac{N^*(T_L + T_{rx,L})}{N_L^* \Delta G} - T_{rx,R} \quad (3\text{-}57)$$

This value of T_{ant} can be tested by viewing at an external target with known characteristics (e.g. Dome-C in Antarctica). If the calibration has been undertaken well, the measurement of T_{ant} at this target is expected to be consistent over time. If it is assumed that T_{ant} is known, then an independent estimate of G_{sys} can be found without using blackbody by:

$$\tilde{G}_{sys} = \frac{N^* L_n}{kB(T_{ant} + \hat{T}_{rx})\Delta G} \quad (3\text{-}58)$$

Once the model parameters and behaviour of G_{sys}, ΔG and T_{rx} are confirmed, the blackbody and/or Antarctic target measurements can be used as independent checks.

3.2.5 GNSS Transmit Power Determination

Surface reflectivity is a ratio of reflected power over incident power. The incident power can be derived by estimating the transmit power towards the specular point.

3.2.5.1 Effective Isotropic Radiated Power (EIRP CM#1: Modelled)

An estimate of the Effective Isotropic Radiated Power (EIRP) at GNSS transmitter (Tx) towards the specular point is calculated. The L1b method models the EIRP based on a model of the transmit power and antenna pattern. The gain of the transmitting antenna (G^t) and transmit power (P_t) is to be found from a lookup table that contains a record of GPS and Galileo transmission data (see AD-4), sourced from either published or learnt data. The Tx antenna gain calculation requires an estimation of the GNSS satellite yaw angle.

EIRP is related to transmitter power as follows in watts, where $G^t(\vartheta, \varphi)$ is the gain of the transmitting antenna and P_t is the transmitted power:

$$EIRP = P_t G^t(\vartheta, \varphi) \quad (3\text{-}59)$$

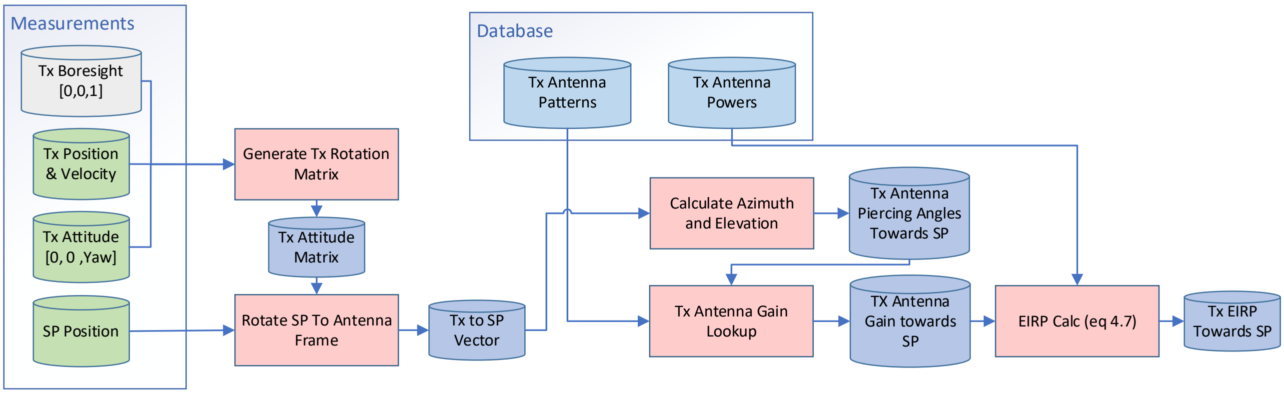

Figure 3.14 EIRP CM#1 Flow Diagram

3.2.5.2 EIRP CM#2 and CM#3

Two further methods of determining transmit power are handled in processor extensions. CM#2 uses *a posteriori* signals reflected off the ocean to generate receiver and transmitter power corrections, described in [RD-13], and CM#3 uses direct signals to calibrate measurements and provides EIRP and reflectivity coefficients in L1b metadata directly, described in Section 3.3 of this document.

3.2.6 Reflectivities

3.2.6.1 Reflection Coefficient

Knowing the power incident at the receiver antenna after coherent reflection by the surface (P_r), the reflection coefficient (equivalent reflectivity) $\Gamma(\vartheta)$ can be determined, where R_r is the range from the receiver to the specular point

(SP), R_t is the range from the transmitter to SP, λ is the signal wavelength, G^t (ϑ) and G^r (ϑ) are the gain of the transmitting and receiving (i.e., down-looking, including input cables) antennas and P_t is the transmitted power (RD-2).

$$P_r = \Gamma(\vartheta)\frac{\lambda^2 G^t(\vartheta)G^r(\vartheta)P_t}{(4\pi)^2(R_r+R_t)^2} \quad (3\text{-}60)$$

3.2.6.2 Normalised Backscatter Radar Cross-Section (NBRCS)

With knowledge of the scattering area, the NBRCS (Bistatic Scattering coefficient, σ^o) can be determined in the case of incoherent scattering (RD-2).

$$P_r = \sigma^o(i,s)\frac{\lambda^2 G^t(\vartheta)G^r(\vartheta)P_t A_S}{(4\pi)^3 {R_r}^2 {R_t}^2} \quad (3\text{-}61)$$

where σ^o is a function of the incidence ***i*** and observation ***s*** directions of the resolution cell. A_S is the area of the resolution cell determined by the range and Doppler discrimination of the system, at a distance from the transmitter and receiver to a point on the surface of the cell. Here it is defined by the 1st iso-range ellipse following [Haff, Zuffada, et al. 2002], the surface covers the specular point delay and an additional delay of one code chip (T_c). T_c is dependent on the signal under test i.e., the chip rate of L1/E1 or L5/E5. The area of the ellipse is estimated as follows:

$$A_S = \pi\frac{1}{\sin\epsilon}\left(\frac{R_r R_t T_c c}{R_r+R_t}\right) \quad (3\text{-}62)$$

The grazing angle (ϵ), is the 90-degree complement to the angle of incidence (i). The speed of light is denoted by c.

3.2.7 Best Calibration Method Estimates

Using CM#1, CM#2 and CM#3 can give three different results for EIRP, reflectivity and NBRCS, so these variables are labelled with the CM used. The best values for EIRP, reflectivity and NBRCS are nominally allocated as follows:

- GPS L1, Galileo E1, LHCP and RHCP – Best EIRP, reflectivity and NBRCS come from using CM#3 (see section 3.3)
- GPS L5, Galileo E5a, LHCP and RHCP – Best EIRP, reflectivity and NBRCS come from using CM#1 (directly tracked L5, E5 signals are currently not available for calibration)

The performance of the Calibration Methods will be assessed, and nominal allocations may change depending on the results achieved in orbit.

3.2.8 Quality Flags

Quality flags carry information that may be of value to users in interpreting science measurements, providing information, warnings, or indicating when measurements are invalid. The baseline quality flags are captured within this section (along with baseline threshold settings) however, the list of flags will continue to be developed and expanded as experience is gathered with data processing from the instrument.

3.2.8.1 DirectSignalinDDM

The direct signal can appear in the processed DDMs, due to being picked up in the side-lobes of the nadir pointing antenna. Taking the GPS C/A signal as an example, the GPS C/A signal repeats every 1023 chips, or 1 ms. This means that the reflected signal, if at a multiple of 1 ms delay from the reflected signal and within the range of processed Doppler frequencies, can be picked up by the DDM matched filtering for the reflection. The other navigation signals that HydroGNSS will be processing (E1B/C, E5a and L5) have different code lengths and rates, which will be satisfactorily accounted for in the calculations. For all signals a 1 chip and 1000 Hz guard region is used, to maintain the separation from the ambiguity function. The full signal parameters are summarised in AD-4, relevant settings for the DirectSignalinDDM algorithm are provided below:

Table 3-7 L1b DirectSignalinDDM Signal Settings

Signal	Freq (MHz)	CODE_RATE (Mcps)	Primary CODE_LENGTH (Chips)	Code Repeat interval
GPS L1 C/A Code	1575.42	1.023	1023	1 ms / 300 km
GPS L5	1176.45	10.23	10230	1 ms / 300 km

Galileo E1 B+C	1575.42	1.023	4092	4 ms / 1200 km
Galileo E5a	1176.45	10.23	10230	1 ms / 300 km

To mark which DDMs are contaminated, a flag is provided in the L1b data. The <DirectSignalInDDM> flag is set to true (1) when the delay and the Doppler of the direct signal are within the extent of the processed DDM.

Two examples of the flag are show in Figure 3.15 and Figure 3.16 taken from RD-3. In these figures, DDMs are made into a montage to display a whole track. Each DDM is put beside the previous (left to right) to complete a row of 50 seconds. The total track length is 261 seconds.

The dashed black line indicates potentially contaminated DDMs. The flag is provided purely by calculation of the relative delay and Doppler, not inspection of the DDM pixels. It could therefore still flag circumstances where there is no visible leakage potentially due to the direct signal being too weak to appear in the DDM, for example if the direct signal were in a null of the nadir antenna gain. Alternatively, it could be due to the direct signal appearing at the edge of DDM Doppler band in which case it would tend to be only weakly visible in the DDM due to the large code rate difference.

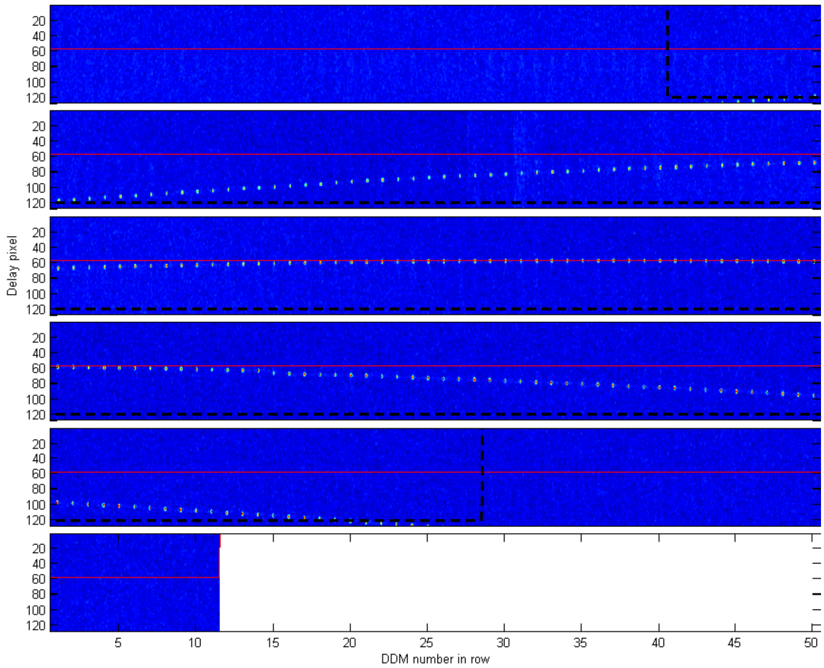

Figure 3.15 A strong direct signal that has been flagged in a partial track. TDS-1 RD84 Track 12

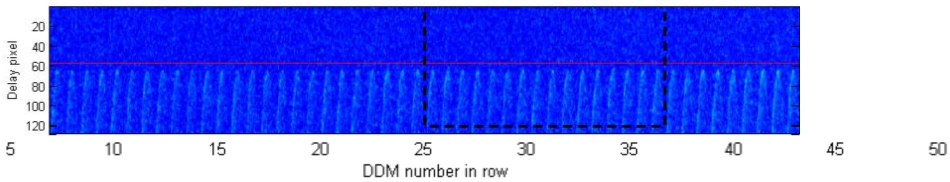

Figure 3.16 Example: flag set but the direct signal is not visible in a partial track. TDS-1 RD84 Track 15

3.2.8.2 SNR Threshold

Two flags are provided <LowSNR> and <VeryLowSNR> These flags notify users when the SNR of a DDM is below a threshold, baseline settings are -2dB and -8dB respectively, and the measurement is not recommended for use. The two flags allow for use with different products. For example, biomass measurements necessarily use signals with low SNR, whereas other products may prefer to use higher values of SNR.

3.2.8.3 Noise Kurtosis:

The kurtosis is added as a quality indicator for the noise measurement. The kurtosis is calculated to find the 'tailedness' or magnitude of the outliers in the chosen noise box which may indicate the presence of RF interference.

The kurtosis measure is the sample excess kurtosis,

$$g_2 = \frac{\frac{1}{n}\sum_{i=1}^{n}(x_i-\bar{x})^4}{\left(\frac{1}{n}\sum_{i=1}^{n}(x_i-\bar{x})^2\right)^2} - 3 \qquad (3\text{-}63)$$

3.2.8.4 Land Type

The <LandType> parameter provides a classification of the land cover at the specular point; this can also be used to determine land or water. The land cover database is a 300m resolution map of latitude and longitude and is obtained from the ESA Land Cover CCI via the following link: https://www.esa-landcover-cci.org

Land types are referenced in Table 3-8:

Table 3-8 Land Type Values

0	No_data	120	Shrubland
10	Cropland_rainfed	121	Shrubland_evergreen
11	Cropland_rainfed_herbaceous_cover	122	Shrubland_deciduous
12	Cropland_rainfed_tree_or_chrub_cover	130	Grassland
20	Cropland_irrigated	140	Lichens_and_mosses
30	Mosaic_cropland	150	Sparse_vegetation
40	Mosaic_natural_vegetation	151	Sparse_tree
50	Tree_broadleaved_evergreen_closed_to_open	152	Sparse_shrub
60	Tree_broadleaved_deciduous_closed_to_open	153	Sparse_herbaceous
61	Tree_broadleaved_deciduous_closed	160	Tree_cover_flooded_fresh_or_brackish_water
62	Tree_broadleaved_deciduous_open	170	Tree_cover_flooded_saline_water
70	Tree_needleleavedleaved_evergreen_closed_to_open	180	Shrub_or_herbaceous_cover_flooded
71	Tree_needleleaved_evergreen_closed	190	Urban
72	Tree_needleleaved_evergreen_open	200	Bare_areas
80	Tree_needleleaved_deciduous_closed_to_open	201	Bare_areas_consolidated
81	Tree_needleleaved_deciduous_closed	202	Bare_areas_unconsolidated
82	Tree_needleleaved_deciduous_open	210	Water
90	Tree_mixed	220	Snow_and_ice
100	Mosaic_tree_and_shrub		
110	Mosaic_herbaceous		

3.2.8.5 AGSP Flag

A low AGSP flag <LowAGSP>, the baseline implementation is set such that points with an AGSP below 5dBi maybe discarded as being too weak for some purposes.

3.2.8.6 Incidence Angle

The point is flagged if the incidence angle is greater than 50 degrees (baseline setting), so that it may be rejected by the user.

3.2.8.7 GNSS Transmitter Yaw Steering Status

The L1b processor does not attempt to model the non-nominal yaw steering behaviour of each GPS block or GNSS constellation. The `GnssTransmitterYaw` parameter provides the modelled nominal yaw angle in all cases and raises a flag if non-nominal behaviour is expected (for example where the Tx transmitter is in the Earth's shadow). The flag is raised during the following conditions:

- The sun elevation beta angle is larger than 4.1degrees
- The collinearity (sun and satellite) angle is more than 10.0 degrees

The flag takes the following values:

- 0: Modified Yaw Steering, non-nominal yaw behaviour expected.
- 1: Nominal Yaw Steering.

3.2.8.8 Overall Quality Flag

Low quality summary flag composed of a bitwise or of VeryLowSNR, LowAGSP, and other flags to be listed. Flag not set (value = zero) means the data is of good quality. When the flag is set (value= 1) then the quality is poor.

3.3 L1B_EXT DIRECT CALIBRATION PROCESSOR (L1BOP-DX)

The SSTL Level1b DX extension processor (L1BOP-DX) generates metadata containing direct transmitter power corrections to allow compensation in reflectivity due to dynamic changes in transmit power, i.e. CM#3. Updated parameters are output as metadata values to accompany DDMs at L1b. A training module (L1BOP-DX-L) is implemented to determine GNSS satellite antenna patterns as new satellites become available.

The SSTL Level1b_ext metadata contains:

1. GNSS satellite transmitter power corrections, based on the GNSS antenna gain pattern, and a comparison of the HydroGNSS zenith black body measurement.
2. Updated EIRP (CM#3), power towards specular point from GNSS transmitter
3. Updated reflectivity (CM#3)
4. Updated sigma-0 (CM#3)

Table 3-9 L1b_EXT processing

Type	Data	Format / units	Note
Inputs:	L1a DDM, Blackbody and metadata files	*.netCDF	HydroGNSS PDGS Algorithm ICD (AD-1)
	L1b metadata	*.netCDF	
	DirectSignal	*.netCDF	
Auxiliary Data	Models of GNSS Transmit antenna patterns derived from learning module	TBD	
Auxiliary Data	Same metadata used in Level 1b for reflection calculations (see previous section)	Misc	Recalculation of Reflection parameters with improved EIRP
Outputs:	EIRP (CM#3) ReflectionCoefficientAtSP (CM#3) Sigma0 (CM#3) Sigma0Area GNSSPowerDensityAtSP	*.netCDF, 1Hz	HydroGNSS PDGS Algorithm ICD (AD-1)

3.3.1 Theoretical Description

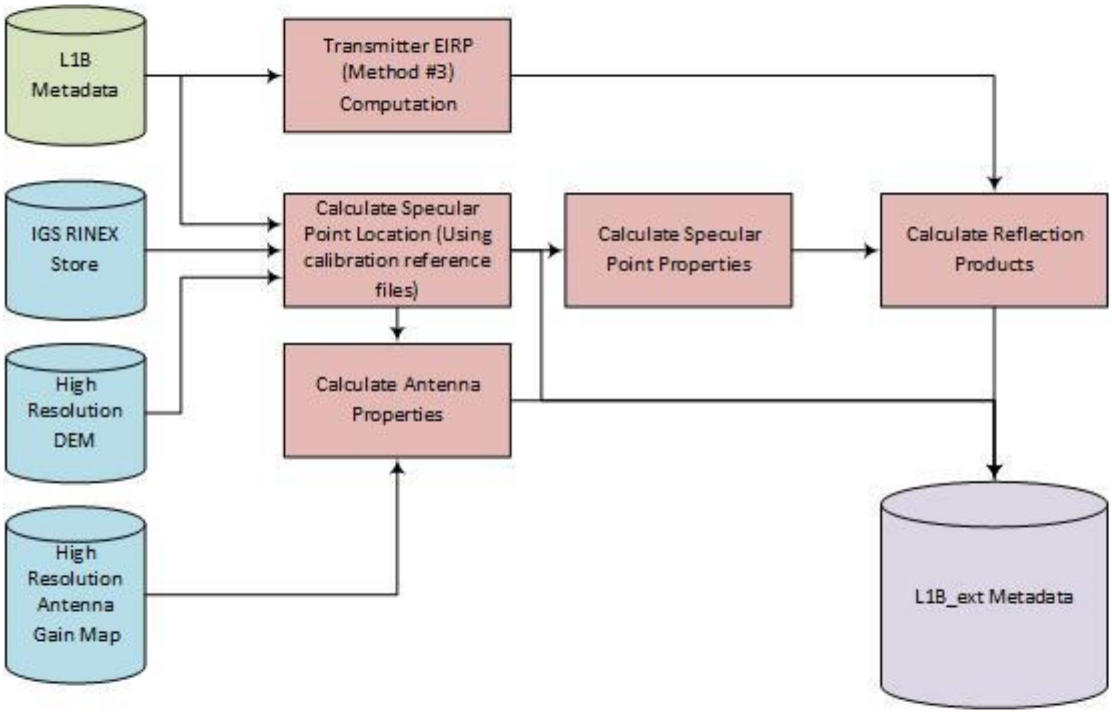

Figure 3.17 L1b_ext Processing

3.3.2 Direct Signal Power

The direct signal power is measured and provided in the "L1a" directSignalPower.nc dataset. The zenith signal measurement is achieved through a closed coherent tracking loop and does not follow the same process as the DDM calculation. The zenith received signal power and noise power are separately made available by the receiver once per second.

Following Section 3.2.4, the <SignalPower> dataset contains the measured signal power (which includes additive noise). The dataset <NoisePower> contains the noise measurement from dedicated Rx channels. A scaling factor is required to convert the zenith navigation correlator count measurement into a level consistent with the DDM counts of the nadir and blackbody (nominal scaling factor of 0.016885709). Similarly to the Nadir correction, to determine the power received at the input to the LNA reference point (P_r^D), correction of the signal minus noise is required to account for the analogue (LNA, C2, FE) and digital (ADC conversion) gains. The direct power is defined as follows:

$$P_r^D = \frac{ScalingFactor(\text{SignalPower}-\text{NoisePower})}{\text{G}_{\text{Sys}}^{\text{D}}} \quad (3\text{-}64)$$

System gain (G_{Sys}^D) is calculated as previous equations using the zenith blackbody terms, $\tilde{G}_{sys} = \frac{N^* L_n}{kB(T_{ant}+\hat{T}_{rx})\Delta G}$ (3-58). Power at the zenith antenna, if required, is determined by consideration of the antenna gain at the receiver to transmitter elevation angle (including the input cable C1).

3.3.3 Effective Isotropic Radiated Power (EIRP CM#3: Direct)

EIRP processing in the L1BOP-DX module uses the direct signal and provides a corrected estimate of the GNSS EIRP towards the specular point. In the simplest form the relative change in transmit power can be used to adjust the received reflected power.

The process for HydroGNSS follows a similar approach to that used by CYGNSS [see T. Wang et al, 2022]:

- Zenith power (P_r^D) at the reference point is calculated in L1b.
- Generate/Recall the ZSR (zenith to specular point ratio as a function of the incidence angle) for the GNSS transmitter in use.
- Calculate the EIRP in the Specular Point direction using the ZSR approximation where R is the range from transmitter to receiver:

$$EIRP = \frac{(4\pi R^2)}{\lambda^2} \frac{P_r^D}{G^r(\vartheta)\ ZSR} \quad (3\text{-}65)$$

The ZSR is a function of the specular incidence angle for each transmitter, where the average value of gain is taken over all azimuth angles. The method allows for ZSR curves to be generated for all satellites where gain maps are available, or where patterns are learnt using the Antenna Pattern Learning Module (L1BOP-DX-L).

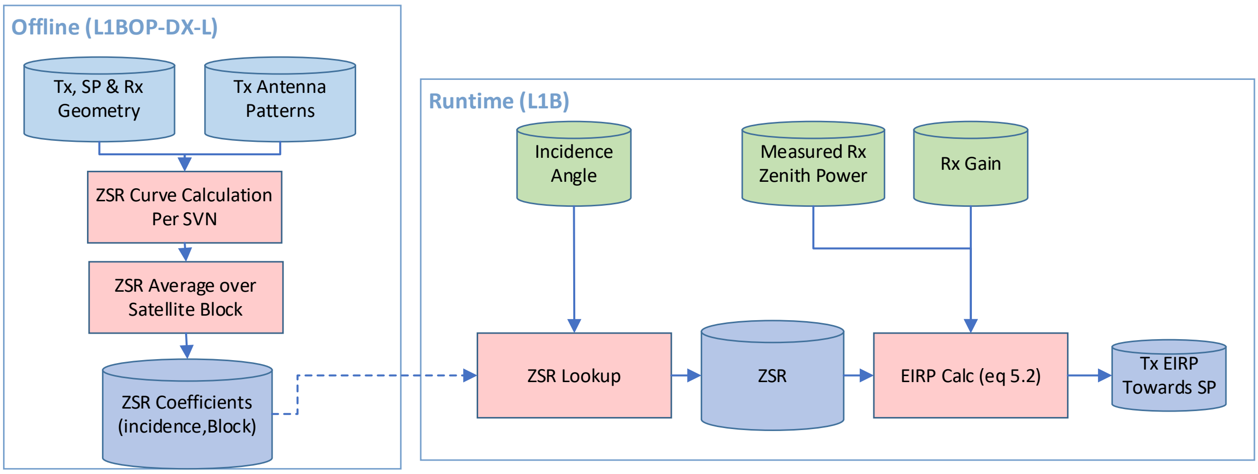

Figure 3.18 EIRP CM#3 Calculation

The ZSR calculation is performed on each antenna pattern as part of the L1BOP-DX-L processor as follows, in this case the published pattern is provided in 10-degree increments over azimuth:

$$ZSR(\theta_{inc}) \approx \frac{1}{36}\sum \frac{G_{Zenith}(\theta_{inc})}{G_{SP}(\theta_{inc})} \tag{3-66}$$

$ZSR(\theta_{inc})$, is the Zenith to Specular Point Ratio approximation expressed as a function of the incidence angle.
$G_{Zenith}(\theta_{inc})$, average value of the antenna gains towards the zenith of all azimuth angles at an incidence angle (θ_{inc}).
$G_{SP}(\theta_{inc})$, average value of the antenna gains towards the specular point of all azimuth angles at an incidence angle (θ_{inc}).

For each execution of L1BOP-DX-L, the processor provides the ZSR curves for each available transmit antenna pattern and transmitter block. These curves can be directly used by the L1b processor for calibration method #3. Plots of individual SVNs show around >0.2dB variation in ZSR between satellites, whereas there is a <0.2dB variation in the ZSR between satellites of the same block. Therefore, there is little benefit from providing a ZSR curve for each SVN. The ZSR curve is provided to the L1B processor as a polynomial function describing the average ZSR for each satellite block, the coefficient order is configurable.

3.3.4 Specular Point

Calculated as L1b.

3.3.5 Reflectivity, NBRCS

Calculated as L1b (section 3.2.6) with corrected EIRP CM#3.

3.4 ANTENNA PATTERN LEARNING PROCESSOR (L1BOP-DX)

The transmit power and pattern of the transmitting antenna is to be found from lookup tables that are learnt from transmitted GNSS signals. Knowledge of the zenith receive antenna pattern is also important to allow estimation of the transmitted power of the GNSS satellites. A processing tool has been developed that can learn these patterns from in-orbit data. Although not part of the main processor, the antenna patterns it produces can be used by the L1 processor operationally. This section summarises the processing tool, derived from the User Manual [RD-16].

This learning will take place at the beginning of the mission and every time there are new GNSS satellites commissioned.

3.4.1 Processing Steps

The processor is intended to operate on direct GNSS measurements from HydroGNSS, but it can also use GNSS data from Sentinel-6 data to learn Galileo E5 patterns. To operate correctly, there are three steps:

Table 3-10 Processing steps: Learn Rx Pattern, Tx Powers and Patterns

Step	Product	Source	Comments
1.	Zenith Rx Pattern: HydroGNSS: L1/E1 Sentinel-6 E5 ref.	HydroGNSS Rx L1 RHCP data. (L5 not available). Sentinel-6 data	One Week of in-orbit data
2.	Tx Patterns: GPS SVNs (L1) Galileo SVNs (E1) Galileo E5	HydroGNSS L1/E1 Sentinel-6	One Month of data for learning entire pattern.
3.	Tx Powers: GPS SVNs (L1) Galileo SVNs (E1) Galileo E5	HydroGNSS L1/E1 Sentinel-6 for E5. L5 not available.	One week of data.

Steps 2 and 3 in particular are hard to decouple, as the power received is a combination of the antenna pattern and the absolute power output. If external reference data can be used to constrain the power, the power estimation step can be bypassed. Similarly, antenna patterns are available, so could be used to constrain the pattern learning step.

3.4.2 Functions

Some of the functions used by the learning tool include:

- Data conversion – allowing inputs of PVT and SNR from different satellite sources, convert to generic file.
- Geometry computation – use of positions to determine range, attitude of transmit and receive antennas.
- Yaw calculation for GNSS satellites is included, nominal and non-nominal determination.
- Power computation – calculation of power at each location and angle
- Allocation and fitting to each of three models: receive pattern, transmit pattern, and transit power.
- Output of antenna pattern to appropriate database.
- ZSR (Zenith to Specular Ratio) tables can be generated from the antenna patterns.

4 VALIDATION / UNCERTAINTY

The calibration validation plan document (AD-3) describes the validation methodology for the L1B processor. L1B validation is performed in comparison to the E2ES. The following section summarises the latest results, refer to the individual test campaign reports for further information and additional results. The E2ES has been validated against CYGNSS and other data sources (RD-10).

The following results are taken from "Test-1b" E2ES run, processed with the latest L1B processor. The simulated error terms are as follows, simulating a zero error (or "noise") and full noise scenario:

Table 4-1: Validation Test Settings

Simulation Settings:	Test 1a (No Noise)	Test 1b (inc. Monte Carlo error contribution)
Mode	Monte Carlo (random error)	Monte Carlo (random error)
Site	San Luis Valley, Entire site (284 points)	San Luis Valley, Entire site (284 points)
Tx Power Error (dBW)	0	0.4
Rx Roll Error (deg)	0	0.55
Rx Pitch Error (deg)	0	0.45
Rx Yaw Error (deg)	0	2
Rx Nominal Pitch Angle (deg)	-20	-20
Noise Figure Error (dB)	0	0.5
Receiver Temp error (K)	0	10
Gain Error (dB)	0	0.4
LNA Noise Figure Constant (gNF)	0	2.33
LNA Gain Gradient (mG)	0	-0.035

4.1 GEOLOCATION

Geolocation implemented in the processor reproduces the instrument calculation of Specular Point. The results agree with the E2ES implementation to ~1 metre. The height retrieval is quantised to 1m (DEM and Geoid). NB neither Level 1 processor nor E2ES applied corrections for surface slope in these tests.

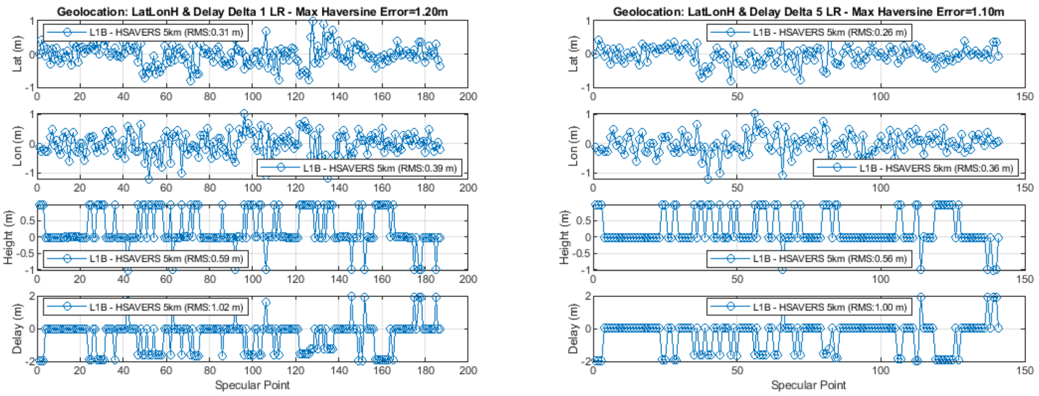

Figure 4.1 L1B Geolocation Comparison against E2ES, Test1a L1 (LHS) and L5 (RHS)

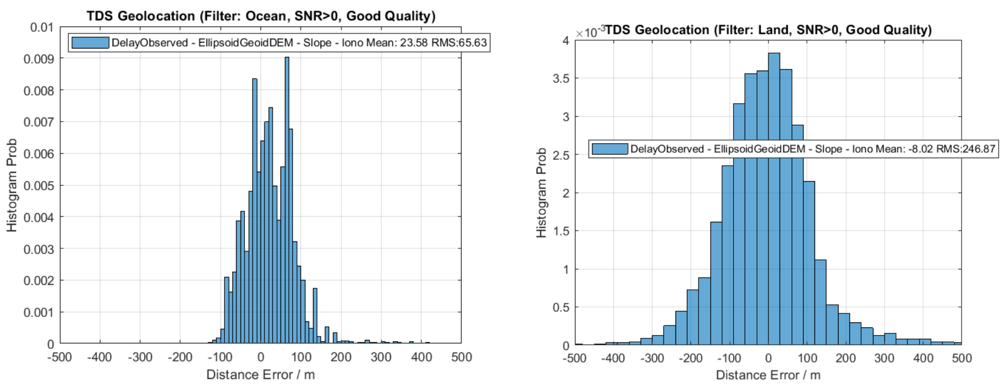

Figure 4.2 L1B Geolocation Comparison against TDS-1 Data, Over ocean (LHS) and Land (RHS)

In Figure 4.2 TDS-1 DDMs from in orbit are used to measure offset from peak signal to Level 1 processor calculated geolocated centre; over ocean, agreement of 66 meters rms was achieved, while 248 metres was achieved over land.

4.2 REFLECTIVITY

Comparison against the E2ES shows agreement in reflectivity to within 0.5dB RMS for both L1 and L5 channels. The CM#3 results use the ZSR method for obtaining the Tx EIRP, rather than the model of the transmitter yaw that is used in CM#1.

CM#3 is not available for L5 due to the instrument not tracking direct L5 signals. Test 1a exhibits noisier results for several tracks in the dataset, due to the lower SNR of those points and higher incidence angles (such results can be flagged and filtered as required). The applied filter for both tests removes points with SNR <-5dB and does not filter for AGSP.

The results of Test 1b contain the combined random errors (Table 4-1) introduced in each processing step: attitude, radiometric calibration, receiver antenna gains and incident power.

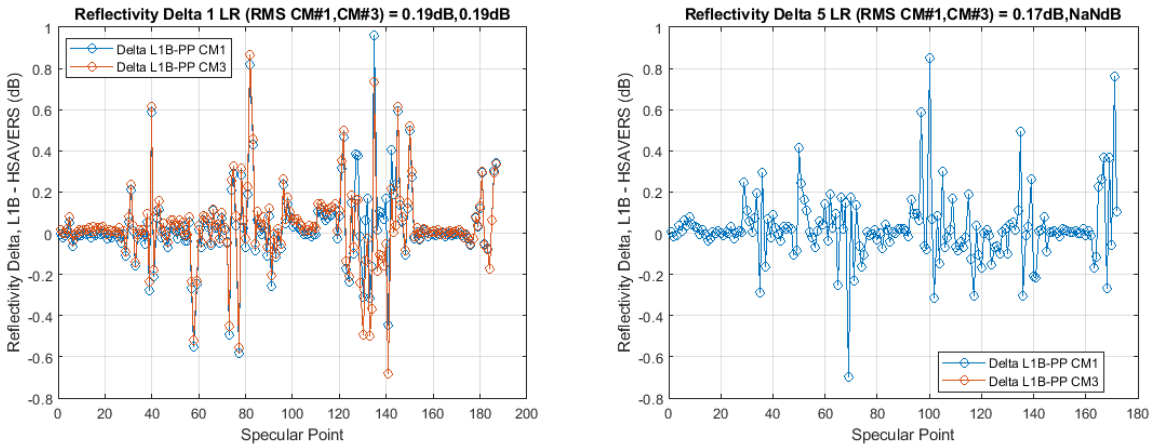

Figure 4.3 L1B Reflectivity Delta against E2ES, Test1a L1 (LHS) and L5 (RHS)

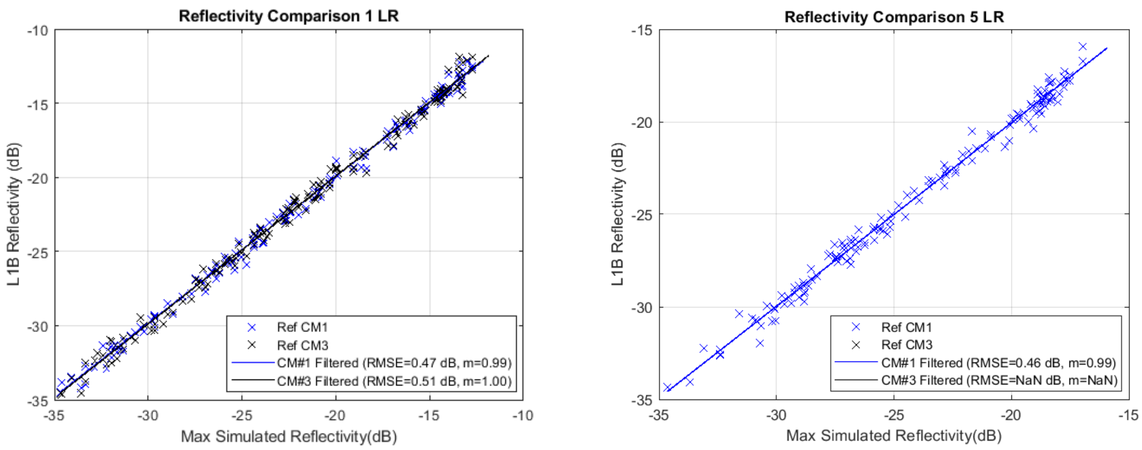

Figure 4.4 L1B Reflectivity Comparison against E2ES, Test1b L1 (LHS) and L5 (RHS)

4.2.1 Example TDS Results

The L1b processor can also be used to process historic TDS-1 data, an example is provided below including both calibration methods.

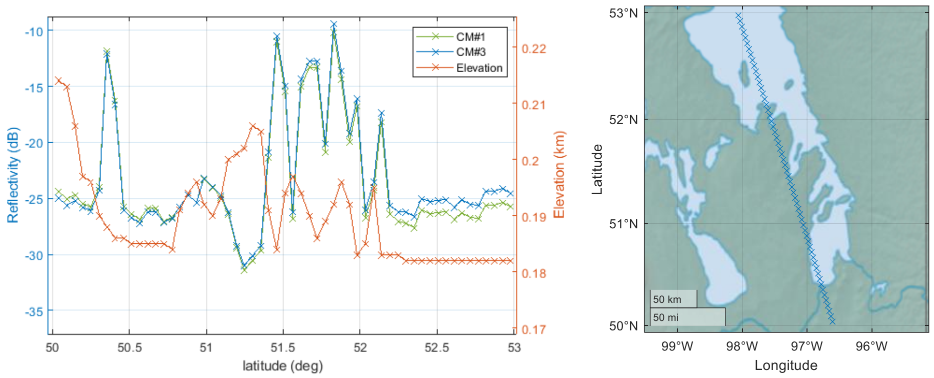

Figure 4.5 L1B Reflectivity Comparison for CM#1 and 3 (TDS-1 2018-08, GPS SVN 60)

4.3 ANTENNA PATTERN AND POWER LEARNING

4.3.1 Receiver antenna pattern learning

Receive antenna patterns are learnt over one week, but in the example shown below (Figure 4.6) data is processed from Sentinel-6 over 24 days to determine the antenna pattern of the receiver. The gain deviation seen is approximately 1 dB for GPS and slightly smaller for Galileo, suggesting that transmit characteristics affect the assessment of the receiver pattern accuracy.

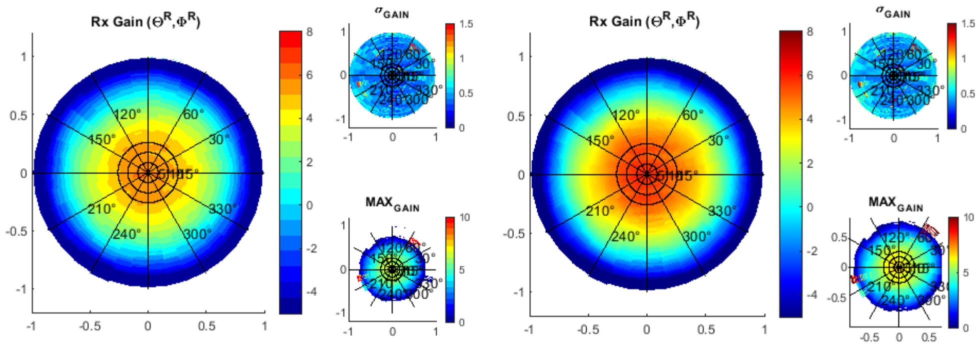

Figure 4.6 Learnt Sentinel-6a GNSS Patterns (in dBi): Galileo E1 (LHS) and E5 (RHS) Rx Patterns

4.3.2 Transmit Power Learning

The measured average power is within 0.5dB of expected values for GPS blocks, although there is a significant deviation visible in GPS Block IIR-M satellites. Flex Power was not documented to be operational during this period (Nov 2022) but may still have been present.

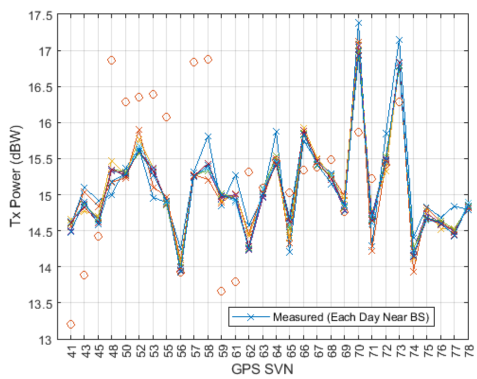

Figure 4.7 S6a L1 Plot: Tx GPS Measured Power Vs. Published Reference Levels (circles)

4.3.3 Transmit Pattern Learning

Using the published transmit powers, the Tx pattern for each SVN is generated. Residuals are low (<1dB) and the patterns shows similarity to the published patterns.

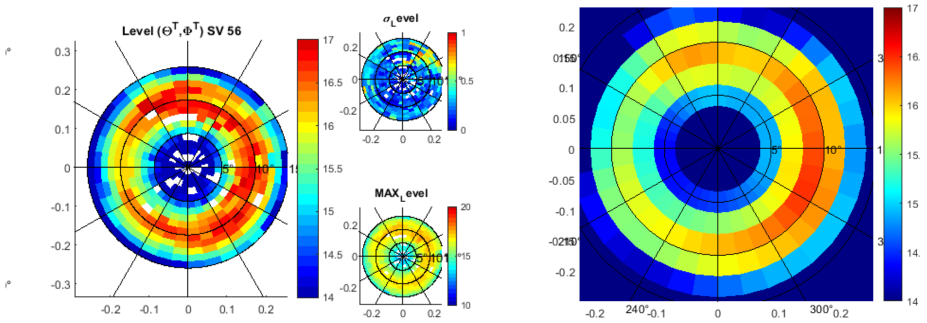

Figure 4.8 Sentinel-6a (in dBi): Tx GPS SVN 56 (BII-M) Measured (LHS) Vs. Published Reference Pattern (RHS)

4.4 UNCERTAINTY

The uncertainty table below is extracted from the calibration and validation document (AD-3), a preliminary allocation of error terms is given assuming the root sum square of terms.

Table 4-2: Reflectivity Error Budget, Allocation of Reflectivity Errors

Parameter	Req: 1 dB		Goal 0.6 dB		Comments
	Target%	Target	Target%	Target	
Receive Power Measurement (Nadir)	10%	0.41 dB	8%	0.33 dB	Accuracy has dependence on reflection strength
Radiometric Calibration (Nadir)	9%	0.37 dB	5%	0.20 dB	Estimate gain & NF (Noise Figure) due to temperature
Antenna gain SP knowledge	8%	0.33 dB	5%	0.21 dB	Smallest near boresight, worse at edge FOV May have calibration corrections in orbit
Antenna gain error due to attitude uncertainty	10%	0.41 dB	6%	0.25 dB	Smallest near boresight
Reflected Power	19% (rss)	0.73 dB	13%(rss)	0.49 dB	
Find EIRP using Calibration Method 3: Receiver power measurement (Zenith)	10%	0.41 dB	5%	0.21 dB	Direct signal tracking loops
Radiometric Calibration (Zenith)	9%	0.37 dB	5%	0.20 dB	Estimate gain & NF due to temperature
Antenna gain knowledge (Zenith)	8%	0.33 dB	4%	0.17 dB	Assume pre-launch pattern
Antenna gain error due to attitude uncertainty	5%	0.21 dB	3%	0.13 dB	Zenith antenna gain has low gradient
EIRP error due to Zenith to Specular	8%	0.33 dB	5%	0.21 dB	Dependence on GNSS Tx pattern knowledge
Incident Power	18% (rss)	0.73 dB	10% (rss)	0.41 dB	
Reflectivity	**26% (rss)**	**1 dB**	**16% (rss)**	**0.63 dB**	Total Error Budget

5 FUTURE WORK

5.1 UPDATES EXPECTED PRIOR TO LAUNCH

Updates anticipated to be made to the L1b processor before launch (or during commissioning) are listed here:

- Quality flags refinements to improve flagging of relevant issues in data
- Antarctic DEM implementation – not relevant for main mission purposes.
- Snow/ice data flag – not currently required by processors.

5.2 AREAS FOR FUTURE ENHANCEMENT

Potential future enhancements to the Level 1 processors (not in current scope) are listed here:

- Alternative DDM signal metrics, include leading, trailing edges, integrated area, and stare processing outputs.
- An additional Land Cover Flag that identifies nearby areas with water bodies that could perturb reflections.
- Improved calibration of nadir antenna gain patterns, and RHCP measurements, using knowledge of polarisation of transmit and receive antennas.
- Characterisation of sampling degradation with adjustable gain scheme seen in orbit.
- Exploitation and calibrated adjustments of coherent channel amplitude outputs
- Experimentation and optimisation of bounding box size to constrain reflectivity measurements vs resolution.
- POD – Precise Orbit Determination to improve satellite position knowledge.
- RFI detection and mitigation to ensure measurements are not corrupted by interferers.
- Incorporation of new signals as and when they become available from in orbit instruments, such as SBAS, QZSS.
- As the reflectivity corresponds to a larger footprint than the 300m resolution of the CCI land cover map it would be possible to check the land cover over a larger area and pick the modal value. Furthermore, a quality flag could be produced that flags highly variable land cover over the footprint.

APPENDIX A.

Appendix A:

A.1 Satellite Attitude and Antenna Gain

A.1.1 Attitude Reference Frames

The orbit-defined coordinate system is a system of coordinates that maintains its orientation relative to the Earth as the spacecraft moves in its orbit. An orthogonal triad of unit vectors denoted $\mathbf{X}_O$, $\mathbf{Y}_0$ and $\mathbf{Z}_O$ defines the reference axes in the orbit-defined coordinate system. This is obtained from the receiver position and velocity in non-inertial, ECEF coordinates, WGS-84, which therefore need a transformation due to the rotating frame using the Earth rotation vector,

$$\mathbf{W_e} = \begin{bmatrix} 0 \\ 0 \\ \theta \end{bmatrix}$$

where θ is the Earth rotation rate, 7.2921158553e-5, rad/s.

The inertial velocity is,

$$\mathbf{V_I} = \mathbf{V} + \mathbf{W}_e \times \mathbf{P}$$

where $\mathbf{P}$ and $\mathbf{V}$ are the ECEF receiver position and velocity respectively. The $\mathbf{Y}_0$ or pitch axis is directed toward the negative orbit normal,

$$\mathbf{Y}_O = \frac{-\mathbf{P} \times \mathbf{V_I}}{|\mathbf{P} \times \mathbf{V_I}|} \quad \textbf{(5.1)}$$

The $\mathbf{Z}_O$ or yaw axis, is directed towards the centre of the Earth (nadir)

$$\mathbf{Z}_O = \frac{-\mathbf{P}}{|\mathbf{P}|} \quad \textbf{(5.2)}$$

The $\mathbf{X}_O$ or roll axis completes the orthogonal set as the along-track vector,

$$\mathbf{X}_O = \mathbf{Y}_O \times \mathbf{Z}_O \quad \textbf{(5.3)}$$

A second set of vectors, $\mathbf{X}_B$, $\mathbf{Y}_B$, $\mathbf{Z}_B$ define a second coordinate system termed the body-fixed coordinate system that is defined relative to the spacecraft body itself. The attitude terms, roll, pitch and yaw are defined as right-handed rotations about the three orbit-defined axes, with roll corresponding to a rotation about the $\mathbf{X}_O$ axis, pitch a rotation about the $\mathbf{Y}_0$ axis and yaw a rotation about the $\mathbf{Z}_O$ axis.

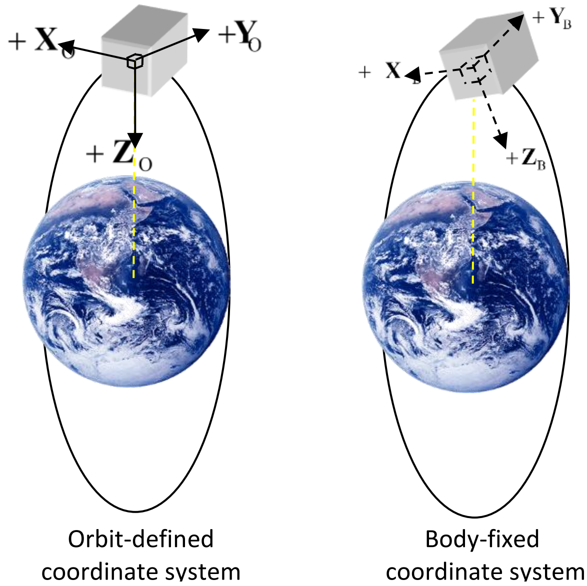

Figure 5-1 Coordinate system definition

The attitude of the spacecraft is the orientation of the body-fixed coordinate system relative to the orbit-defined coordinate system.

A.1.2 Attitude Representations

A common method for describing the attitude of a rigid body is the *direct cosine matrix* or *attitude matrix*. This matrix is a coordinate transformation matrix that maps vectors from the reference frame to the body frame. If $\mathbf{a}_O$ is a vector with components a_1, a_2 and a_3 in the orbit-defined coordinate system, then

$$\mathbf{A}\mathbf{a}_O = \begin{bmatrix} u_1 & u_2 & u_3 \\ v_1 & v_2 & v_3 \\ w_1 & w_2 & w_3 \end{bmatrix} \begin{bmatrix} a_1 \\ a_2 \\ a_3 \end{bmatrix} = \begin{bmatrix} a_u \\ a_v \\ a_w \end{bmatrix} = \mathbf{a}_B \qquad (5.4)$$

where $\mathbf{a}_B$ is the same vector in body-fixed coordinates.

The direct cosine matrix can be parameterised in terms of three rotation angles, commonly known as Euler angles. This allows the orientation of the spacecraft to be defined in terms of three angles: roll, pitch and yaw as defined in the explanation of the coordinate systems above. The spacecraft body-fixed coordinate system is rotated to the orbit-defined coordinate system using three consecutive right-hand positive rotations.

The rotations are defined about the three axes $\mathbf{X}_O$, $\mathbf{Y}_0$ and $\mathbf{Z}_O$, and can be described by the following rotation matrices:

$$\mathbf{R}_X(\phi) = \begin{bmatrix} 1 & 0 & 0 \\ 0 & \cos\phi & \sin\phi \\ 0 & -\sin\phi & \cos\phi \end{bmatrix} \qquad (5.5)$$

$$\mathbf{R}_Y(\theta) = \begin{bmatrix} \cos\theta & 0 & -\sin\theta \\ 0 & 1 & 0 \\ \sin\theta & 0 & \cos\theta \end{bmatrix}$$

$$\mathbf{R}_Z(\psi) = \begin{bmatrix} \cos\psi & \sin\psi & 0 \\ -\sin\psi & \cos\psi & 0 \\ 0 & 0 & 1 \end{bmatrix}$$

where ϕ, θ and ψ represent the rotation angles about the roll, pitch, and yaw axes respectively. These rotation matrices can be combined into a single matrix by finding their product. There are six permutations. The current method is to use the 1-2-3 sequence defined by a rotation ϕ about the roll axis $\mathbf{X}_O$, followed by a rotation θ about the pitch axis $\mathbf{Y}_0$, followed by a rotation ψ about the yaw axis $\mathbf{Z}_O$.

This gives:

$$\boldsymbol{A}_{123}(\varphi,\theta,\psi) = \boldsymbol{R}_Z(\psi)\boldsymbol{R}_Y(\theta)\boldsymbol{R}_X(\varphi) \quad \textbf{(5.6)}$$

Or:

$$\boldsymbol{A} = \begin{bmatrix} \cos\theta\cos\psi & \cos\varphi\sin\psi + \sin\varphi\sin\theta\cos\psi & \sin\varphi\sin\psi - \cos\varphi\sin\theta\cos\psi \\ -\cos\theta\sin\psi & \cos\varphi\cos\psi - \sin\theta\sin\theta\sin\psi & \sin\varphi\cos\psi + \cos\varphi\sin\theta\cos\psi \\ \sin\theta & -\sin\varphi\cos\theta & \cos\varphi\cos\theta \end{bmatrix} \quad \textbf{(5.7)}$$

There is a two-fold ambiguity in ϕ, corresponding to sin ϕ being positive or negative. This ambiguity is resolved by choosing 0 <= ϕ <180 degrees, which allows θ and ψ to be determined uniquely (modulo 360 degrees) unless ϕ is a multiple of 180 degrees when only the sum or difference of θ and ψ can be determined.

A.1.3 Antenna Reference Frame

The antenna reference frame is related to the satellite body frame through a rotation. The rotation allows off-pointing of the mounting of the antenna on the satellite structure. The definition of this rotation allows for a roll about the $\mathbf{X}_B$ axis, which is parameterised by the antenna boresight unit vector $\mathbf{A}_B$.

This coordinate transformation matrix, $\mathbf{A}_R$, maps vectors from the body frame to the antenna reference frame. The antenna reference frame is defined as the right-handed orthogonal frame consisting of the basis vectors: $\mathbf{X}_A$ which is the same as the body-frame $\mathbf{X}_B$, $\mathbf{Z}_A$ which is the antenna boresight vector, $\mathbf{A}_B$, and completing the set, $\mathbf{Y}_A$ which is the vector $v = \mathbf{A}_B \times \mathbf{X}_B$

If $\mathbf{a}_B$ is a vector with components a_1, a_2 and a_3 in the body frame, then the rotation

$$\mathbf{A}_R\mathbf{a}_B = \begin{bmatrix} 1 & 0 & 0 \\ v_1 & v_2 & v_3 \\ A_{B1} & A_{B2} & A_{B3} \end{bmatrix} \begin{bmatrix} a_1 \\ a_2 \\ a_3 \end{bmatrix} = \begin{bmatrix} a_u \\ a_v \\ a_w \end{bmatrix} = \mathbf{a}_A \quad \textbf{(5.8)}$$

gives $\mathbf{a}_A$, which is the same vector in the antenna reference frame, with components a_u, a_v, and a_w

The antenna boresight for TDS-1 is along the $\mathbf{Z}_B$ axis,

$$\mathbf{A}_B = \begin{bmatrix} 0 \\ 0 \\ 1 \end{bmatrix}$$

The antenna boresight for TDS-1 zenith antenna is anti the $\mathbf{Z}_B$ axis,

$$\mathbf{A}_B = \begin{bmatrix} 0 \\ 0 \\ -1 \end{bmatrix}$$

Therefore, the antenna reference frame is equivalent to the satellite body frame.

To determine the antenna gain related to a particular vector, an Antenna Gain Map (AGM) look-up table is indexed into using the vector's azimuth and elevation. For example, the vector $\mathbf{a}_{\mathrm{A}}$, in the antenna reference frame has azimuth angle from the $\mathbf{x}_{\mathrm{A}}$ axis towards the $\mathbf{y}_{\mathrm{A}}$ axis.

$$\varphi_A = \tan(a_v / a_u) \tag{5.9}$$

Where azimuth, φ_A, is taken from -180 to 180 degrees.

Elevation is the angle between the vector and the $\mathbf{z}_{\mathrm{A}}$ axis,

$$\theta_A = \sin(a_w / |\mathbf{a}|) \tag{5.10}$$

Appendix B:

B.1 Delay Doppler Map

B.1.1 DDM Scale

This process is taken from MERRByS Manual [RD-3] applied to TDS-1 data. HydroGNSS is expected to be able to centre the Specular Point in the DDM window using the on-board DEM, therefore this section is provided for information only and may be removed in future.

The DDM processing window is targeted to the specular point using open-loop tracking. The specular point location is calculated on-board, and this is used to determine the delay and Doppler targeted by the DDM window. This is open loop as information from the DDM pixels is not fed back to keep the reflection aligned with the tracking point. The purpose of the reflection targeting is to keep the specular point at a constant, defined, tracking offset in the DDM window. This tracking point is configurable in the receiver, so is reported in the ***<L1bMetadata, Attributes>***.

Delay:

If the DDM has delay pixels numbered with index, *d*, from 0 to ***<NumberOfDelayPixels-1>***. Then the delay scale can be calculated as:

(Delay in samples) =
*d ** ***<CodeDelaySpacingSamplesBetweenPixels [samples / pixel]>***

(Delay in seconds) =
(Delay in samples) / ***<SamplingFrequency [Hz]>***

These give the delay scale from the first row of the DDM.

The location of the tracking point is then defined on this scale as:

(Delay of tracking point in seconds) =
(<TrackingOffsetDelayNs> – <SpecularPathRangeOffset [ns]>) $\times 10^{-9}$

Where ***<TrackingOffsetDelayNs>*** is defined once for a whole track in ***<TrackMetaDataFile, Header>*** and the field ***<SpecularPathRangeOffset>*** is defined per DDM in ***<TrackMetaDataFile, Data Array>***.

This can alternatively be expressed in as the pixel offset from delay row 1. This is in ***<TrackingOffsetDelayInPixels>***, which is calculated as *:*

(Delay Offset of Tracking Point) =
(***<TrackingOffsetDelayNs [ns]>*** / ***<DelayResolution [ns/pixel]>)***

(Delay Offset of Tracking Point Corrected)
= (Delay Offset of Tracking Point)
- (***<SpecularPathRangeOffset[ns]>*** / ***<DelayResolution [ns/pixel]>)***

Note that as this is an offset from pixel 1, a value of 64 in ***<TrackingOffsetDelayInPixels>*** corresponds to the 65th delay row.

Doppler:

For the Doppler scale, the Doppler pixels are indexed D from:
–floor(***<NumberOfDopplerPixels>*** / 2) to + floor((***<NumberOfDopplerPixels>*** - 0.5) / 2)

e.g., for 20 pixels (the bin selection is historical and is not expected to change for HydroGNSS):
-10, -9, -8, -7, -6, -5, -4, -3, -2, -1, 0, 1, 2, 3, 4, 5, 6, 7, 8, 9

The Doppler scale is then,

(Doppler in Hz) =

D × ***<DopplerResolution> - <TrackingOffsetDopplerHz>***

Alternatively, the column, D, targeted is found from:

(Doppler column from tracking point) =

D - ***<TrackingOffsetDopplerInPixels>***

Power:
The DDM pixels are the raw counts from the ZTC unit. Due to the scaling in the processor, these are an arbitrary ‘counts’ unit. The scaling does not change.

B.1.2 ADC Metrics

This process is taken from MERRByS Manual [RD-3] applied to TDS-1 data and will be adapted for HydroGNSS specifics. We use different metrics to measure the quantisation of the front-end ADC sample distributions. These are defined here, and then these metrics are shown for the various SGR-ReSI boards.

The 2-bit ADC produces 4 states [-3, -1, +1, +3]. The number of samples in each of the 4 quantisation states is counted over all the samples in a 100 ms period. They are reported in Packet 74 and called here:

```
adcMinus3Count, adcMinus1Count, adcPlus1Count, adcPlus3Count
```

The total number of samples counted is,

```
totalCounts = adcMinus3Count + adcMinus1Count + adcPlus1Count + adcPlus3Count
```

The sum of all the samples is,

```
totalSum = (3*adcPlus3Count + adcPlus1Count) - (-3*adcMinus3Count -1*adcMinus1Count).
```

We then take the counts to form the “Percent Positive”, “Percentage Magnitude” and “DC Offset” metrics.

The measure of the number of samples that fall in the magnitude bit,

```
“Percentage Magnitude” = ((adcPlus3Count + adcMinus3Count)) / totalCount * 100;
```

A measure of the number of samples that are positive, weighted by their magnitude,

```
“Percent Positive” = (3*adcPlus3Count + adcPlus1Count) / totalSum * 100;
```

The offset in units of the ADC’s Least Significant Bit [LSB]

```
“DC Offset” = totalSum / totalCount;
```

Appendix C:

C.1 Channel Allocation Algorithm

For reference, this is a summary of the allocation algorithm implemented on the SGR-ReSI Instrument that selects the (nominally) four best reflections for processing. AGSP (Antenna Gain at Specular Point) is calculated for both GPS and Galileo satellites based on the on-board receiver antenna gain map (L1) and used as the figure of merit for allocation.

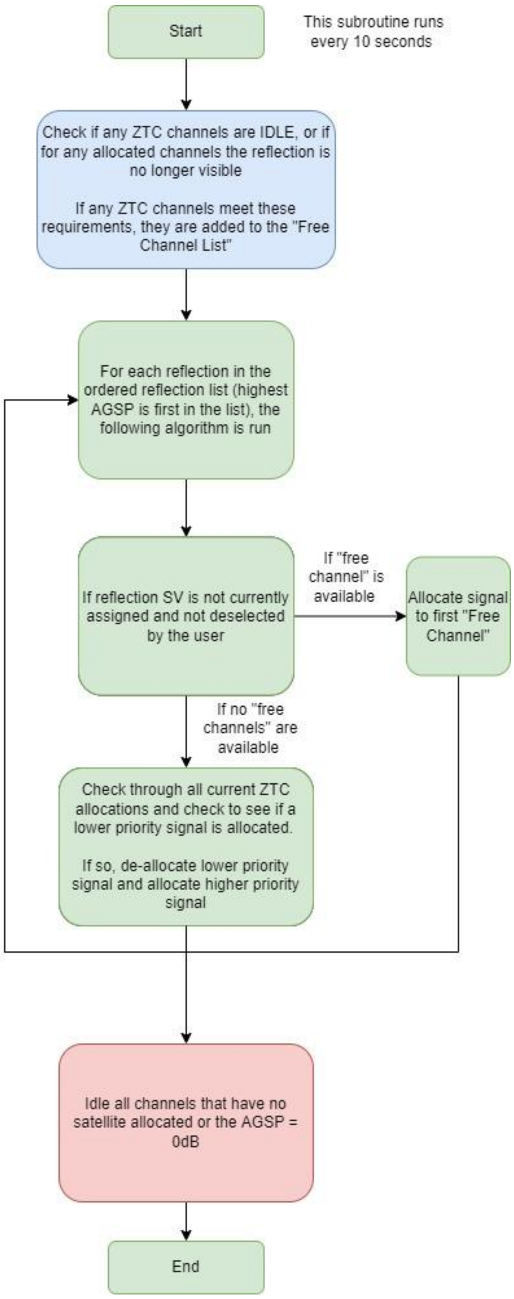

Figure 5.2 Outline of Reflection Allocation Algorithm

There are 16 ZTC channels available in the instrument. When a reflection is allocated, the first two channels are allocated to L1/E1 Left and Right signals. If the satellite indicates it supports L5, two more channels are allocated for the L5/E5a Left and Right signals. All Galileo satellites transmit E5a signals but, at time of writing, only 50% of GPS satellites transmit L5 signals. This means that an additional 5th reflection may be tracked (although only L1 channels may be collected from the 5th reflection). Direct L5/E5a signals are currently acquired and used by the instrument solely to provide data wipe-off on the L5/E5 DDMs, and if direct L5 signals are lost, ZTC measurements are filtered out, and the allocation scheme falls back on L1 tracking. To reduce download of DDMs with no signal present, an antenna gain threshold is defined (e.g. -2 dBi) below which channels will not be allocated and output data.